

Measurement of the Core-collapse Progenitor Mass Distribution of the Small Magellanic Cloud

Katie Auchettl^{1,2,6}, Laura A. Lopez^{1,3,6}, Carles Badenes⁴, Enrico Ramirez-Ruiz^{5,6}, John F. Beacom^{1,2,3}, and Tyler Holland-Ashford^{1,3}

Center for Cosmology and AstroParticle Physics (CCAPP), The Ohio State University, 191 W. Woodruff Ave., Columbus, OH 43210, USA

 Department of Physics, The Ohio State University, 191 W. Woodruff Ave., Columbus, OH 43210, USA
 Department of Astronomy, The Ohio State University, 140 West 18th Avenue, Columbus, OH 43210, USA

 Department of Physics and Astronomy, University of Pittsburgh, 3941 O'Hara Street, Pittsburgh, PA 15260, USA

 Department of Astronomy and Astrophysics, University of California, Santa Cruz, CA 95064, USA
 DARK, Niels Bohr Institute, University of Copenhagen, Lyngbyvej 2, Copenhagen, 2100, Denmark

 Received 2018 May 4; revised 2018 November 18; accepted 2018 November 21; published 2019 January 22

Abstract

The physics of core-collapse (CC) supernovae (SNe) and how the explosions depend on progenitor properties are central questions in astronomy. For only a handful of SNe, the progenitor star has been identified in pre-explosion images. Supernova remnants (SNRs), which are observed long after the original SN event, provide a unique opportunity to increase the number of progenitor measurements. Here we systematically examine the stellar populations in the vicinities of 23 known SNRs in the Small Magellanic Cloud (SMC) using the star formation history (SFH) maps of Harris & Zaritsky. We combine the results with constraints on the SNR metal abundances and environment from X-ray and optical observations. We find that 22 SNRs in the SMC have local SFHs and properties consistent with a CC explosion, several of which are likely to have been high-mass progenitors. This result supports recent theoretical findings that high-mass progenitors can produce successful explosions. We estimate the mass distribution of the CC progenitors and find that this distribution is similar to a Salpeter IMF (within the uncertainties), while this result is shallower than the mass distribution found in M31 and M33 by Jennings et al. and Díaz-Rodríguez et al. using a similar approach. Additionally, we find that a number of the SMC SNRs exhibit a burst of star formation between 50 and 200 Myr ago. As these sources are likely CC, this signature may be indicative of massive stars undergoing delayed CC as a consequence of binary interaction, rapid rotation, or low metallicity. In addition, the lack of Type Ia SNRs in the SMC is possibly a result of the short visibility times of these sources, as they may fall below the sensitivity limits of current radio observations.

Key words: galaxies: individual (Small Magellanic Cloud) – galaxies: star formation – galaxies: stellar content – ISM: supernova remnants – stars: massive – supernovae: general

1. Introduction

One of the most uncertain aspects of stellar evolution is the link between the nature of supernovae (SNe) and their progenitor stars. Generally, it is thought that massive stars $(\gtrsim 8\,M_{\odot})$ undergo core collapse (CC; e.g., Iben 1974; Woosley et al. 2002; Eldridge & Tout 2004; Smartt 2009; Jennings et al. 2012; Ibeling & Heger 2013; Díaz-Rodríguez et al. 2018) once nuclear burning has led to an iron core, and their explosions are driven by a combination of neutrino heating, turbulence, and convection (e.g., reviews by Müller 2016 and Janka 2017, as well as Murphy et al. 2013; Couch & Ott 2015; Dolence et al. 2015; Wongwathanarat et al. 2015). However, the type of SN explosion (i.e., Type Ib, Ic, and II; see review by, e.g., Gal-Yam 2017) is expected to depend strongly on the mass of the progenitor (e.g., Woosley et al. 2002; Heger et al. 2003), whether it is found in a binary (De Donder & Vanbeveren 1998; Izzard et al. 2004; Zapartas et al. 2017), factors such as the metallicity and rotation of the progenitor star (e.g., Heger et al. 2003; Eldridge & Tout 2004; Thompson et al. 2005; Fryer et al. 2012; Kochanek et al. 2017), or a combination of all of these effects (Hirschi et al. 2005; Hirschi 2007; Eldridge et al. 2008, 2017). As such, it is difficult for current theory to confidently predict which stars undergo CC and produce an SN of a given type and which produce a neutron star or a black hole (e.g., Ugliano et al. 2012; Sukhbold & Woosley 2014; Sukhbold et al. 2016; Ebinger et al. 2018).

There have been a number of attempts to identify the progenitor stars of CC SNe in preceding space- and ground-based images (see reviews by Smartt 2009, 2015 and references therein). However, even though direct imaging addresses the above challenges, this method is limited by a number of factors, including the SN rate in the local universe and the depth of archival and/or current observations. Consequently, only a handful of SNe have detections of their progenitor stars (see, e.g., review by Smartt 2015 and studies such as Adams & Kochanek 2015; Gerke et al. 2015; Fox et al. 2017; Van Dyk et al. 2018).

Supernova remnants (SNRs), structures resulting from SNe that occurred hundreds or thousands of years ago, provide us with a unique opportunity to greatly increase the number of explosions with progenitor constraints. The most common method used to link SNRs to their explosions is to estimate metal abundances based on X-ray emission-line strengths and compare these values to those predicted in SN models of different mass progenitors (see, e.g., Badenes et al. 2006; Patnaude et al. 2015; Yamaguchi et al. 2015). In rare cases, light echoes from the originating SNe associated with young SNRs can be observed, providing more information about the progenitor (e.g., Rest et al. 2005, 2008b, 2008a).

Another approach is to characterize progenitor properties of SNRs by examining the resolved stellar populations in their proximity (e.g., Badenes et al. 2009; Jennings et al. 2012, 2014;

Díaz-Rodríguez et al. 2018). These works exploit the campaigns to probe the star formation histories (SFHs) across nearby galaxies, such as the Large Magellanic Cloud (LMC), M31, and M33 (e.g., Harris & Zaritsky 2004, 2009; Lewis et al. 2015). This approach provides a nearly complete (up to $\sim\!70\%$) view of the SN progenitors that exploded in these galaxies (see detailed study by Sarbadhicary et al. 2017), which is important for characterizing SN rates in the Local Group and how they vary in different galactic environments (e.g., with metallicity).

Combining these two methods, Badenes et al. (2009) used the SFH maps of the LMC by Harris & Zaritsky (2009) to estimate the progenitor ages and masses of four CC SNRs and four Type Ia SNRs. They found that their sample of CC SNRs is associated with vigorous star formation (SF) within the last few Myr. However, Type Ia SNRs, which result from the thermonuclear explosion of a white dwarf (WD) in a binary system with either a nondegenerate companion star (singledegenerate scenario) or another WD (double-degenerate scenario; see review by, e.g., Maoz et al. 2014), are located in a wide range of environments, including both old, metalpoor populations and recent highly star-forming regions. Generally, the presence (or lack) of recent SF around a given SNR tentatively suggests a CC (Type Ia) origin, although the averaged SFHs derived from resolved stellar populations in SNR vicinities can be misleading, especially for Type Ia SNRs. However, when combined with constraints on the SNR metal abundances and environment, the local SFHs at the sites of SNRs are a useful, complementary tool to gain insights about the SN progenitors.

In this paper, we examine the SFH maps of the Small Magellanic Cloud (SMC) derived by Harris & Zaritsky (2004) at the sites of the 23 known SNRs in that galaxy (Badenes et al. 2010). Combined with constraints on the metal abundances and environment of each SNR derived from optical and X-ray observations, we attempt to connect the SNR to its progenitor. The paper is organized as follows. In Section 2, we summarize the properties of the SMC and review its known SNRs. In Section 3, we discuss the SFH map of the SMC derived by Harris & Zaritsky (2004) and the galaxy's SFH as a whole. In Section 4, we outline the selection criteria we used to choose our sample. In Section 5, we examine the SFHs around each SNR in our sample and compare them to the properties of the SNe derived from the SNRs themselves. In Section 6, we discuss these results in the context of our understanding of the progenitors of SNe, and in Section 7, we present our conclusions. Appendix A summarizes the observational properties of each SNR as a resource for the reader.

2. The SMC and Its SNRs

The SMC is a close (\sim 61 kpc away; Hilditch et al. 2005), metal-poor galaxy (with $Z_{\rm SMC} \sim Z_{\odot}/5$; Dufour 1984; Russell & Dopita 1992) with active SF (Wilke et al. 2004; Bolatto et al. 2011; Skibba et al. 2012). The SMC has a diverse population of 23 SNRs that have been identified at several wavelengths (Badenes et al. 2010; Temim et al. 2015), and extensive work has gone into characterizing the properties and nature of these sources (e.g., van der Heyden et al. 2004; Haberl et al. 2012a; Lopez et al. 2014a; Takeuchi et al. 2016). In Figure 1, we plot as a green diamond and cyan circles the positions of all 23 SNRs on a continuum-subtracted H α image of the SMC from the Magellanic Cloud Emission Line Survey (MCELS;

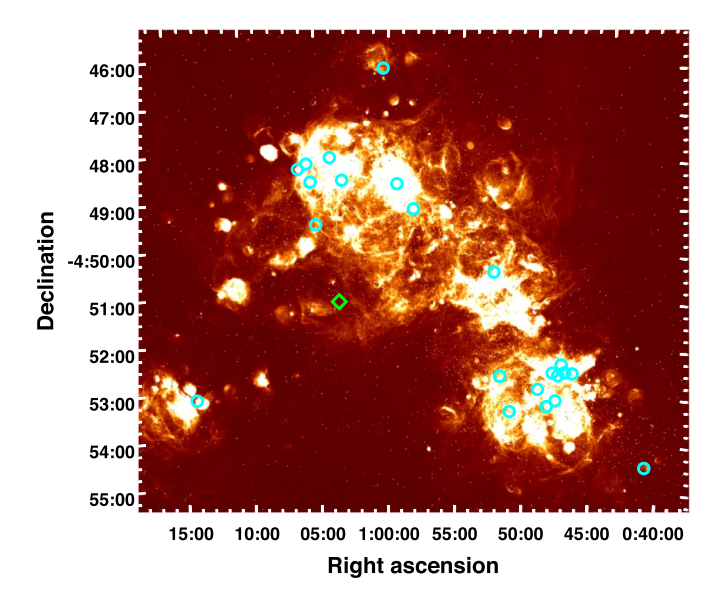


Figure 1. Continuum-subtracted H α image of the SMC from MCELS (Smith & MCELS Team 1999; Winkler et al. 2015). The cyan circles marking the locations of the 22 SMC SNRs that are based on our analysis have SFHs and properties consistent with that of a CC progenitor. The green diamond marks the position of HFPK 334, whose SFH and properties seem to imply a possible Type Ia progenitor (see Section 5 for more details).

Smith & MCELS Team 1999; Winkler et al. 2015). In Table 1, we list the sources' names, positions, and suggested explosive origin. In Appendix A and B, we collate and summarize the properties of each remnant as presented in the literature, providing an up-to-date review of all known SNRs in the SMC. These characteristics are used later in this paper to verify the classification of these sources as either Type Ia or CC based on their SFHs.

Of these remnants, four have possible evidence for Type Ia explosive origins presented in the literature (IKT 4 [SNR J0048.4-7319], IKT 5 [SNR 0047-73.5], IKT 25 [SNR 0104 -72.3], and DEM S128 [SNR 0103-72.4]) based on strong Fe-L emission in their X-ray spectra (van der Heyden et al. 2004). However, others have argued that their environments and intermediate-mass element abundances are more consistent with CC SNR models (e.g., Lopez et al. 2014a). Out of the 23 SMC SNRs, eight have evidence for CC origin (e.g., enhanced intermediate-mass element abundances, detection of a pulsar): DEM S32 [SNR J0046.6-7309], IKT 2 [B0045-73.4], HFPK 419 [SNR J0047.7-7310], IKT 6 [B0049-73.6], IKT 7 [SNR J0051.9-7310], IKT 16 [SNR J0058.3-7218], B0102 -7219 [SNR 0102-72.3], and IKT 23 [SNR 0103-72.6]. The other 11 SNRs identified in the SMC do not have explosion classifications (as Type Ia or CC) in the literature.

Out of the 23 SNRs in the SMC, IKT 25 is the only source where the SFH has been used to constrain the progenitor. Lopez et al. (2014a) found that the peak star formation rate (SFR) at the site of IKT 25 is consistent with a progenitor of a mass \sim 20–40 M_{\odot} . This result was consistent with the intermediate-mass element abundances and the morphological characteristics found using deep *Chandra X-ray Observatory* observations.

3. SFH of the SMC

In this paper, we exploit the SFH map of the SMC from Harris & Zaritsky (2004). Using *UBVI* stellar photometry of

Table 1
SMC SNRs and Their Literature-suggested Origins

Name	Alternative Name	R.A. (J2000)	Decl. (J2000)	Diameter (arcsec)	Suggested SNe Origin	Reference
DEM S5	B0039-7353, HFPK 530, SNR J0040.9-7337	00 ^h 40 ^m 55 ^s	$-73^{d}36^{m}55^{s}$	121	?	
DEM S32	SNR J0046.6-7309	$00^{h}46^{m}39^{s}$	$-73^{d}08^{m}39^{s}$	136	CC	[1]
IKT 2	SNR J0047.2-7308, HFPK 413, B0045-73.4	$00^{h}47^{m}12^{s}$	$-73^{d}08^{m}26^{s}$	66	CC	[1]
B0045-733	HFPK 401, SNR J0047.5-7306	$00^{h}47^{m}29^{s}$	$-73^{d}06^{m}01^{s}$	180	?	
HFPK 419	SNR J0047.7-7310	$00^{h}47^{m}41^{s}$	$-73^{d}09^{m}30^{s}$	90	CC	[1]
NS 21	DEM S35, SNR J0047.8-7317	$00^{h}47^{m}48^{s}$	$-73^{d}17^{m}27^{s}$	76	?	
NS 19	DEM S31, SNR J0048.1-7309	$00^{h}48^{m}06^{s}$	$-73^{d}08^{m}43^{s}$	79	?	
IKT 4	HFPK 454, SNR J0048.4-7319	$00^{h}48^{m}25^{s}$	$-73^{d}19^{m}24^{s}$	84	Ia	[1]
IKT 5	DEM S49, HFPK 437, SNR 0047-73.5, SNR J0049.1-7314	$00^{h}49^{m}07^{s}$	$-73^{d}14^{m}05^{s}$	116	Ia/CC	[1, 2, 3]
IKT 6	1E 0049.4-7339, HFPK 461, B0049-73.6, SNR J0051.1-7321	$00^{h}51^{m}07^{s}$	$-73^{d}21^{m}26^{s}$	144	CC	[1, 4, 5]
IKT 7	HFPK 424, SNR J0051.9-7310	$00^{h}51^{m}54^{s}$	$-73^{d}10^{m}24^{s}$	97	CC	[6]
B0050-728	DEM S68SE, HFPK 285, SNR J0052.6–7238, SNR J005240–723820, SMC 258, NS76	00 ^h 52 ^m 33 ^s	$-72^{d}37^{m}35^{s}$	323	?	
IKT 16	HFPK 185/194, SNR J0058.3-7218	$00^{h}58^{m}16^{s}$	$-72^{d}18^{m}05^{s}$	200	CC	[7, 8]
IKT 18	1E 0057.6-7228, HFPK 148, SNR J0059.4-7210	$00^{h}59^{m}25^{s}$	$-72^{d}10^{m}10^{s}$	158	CC	[9]
DEM S108	B0058-71.8, HFPK 45, SNR J0100.3-7134	$01^{h}00^{m}21^{s}$	$-71^{d}33^{m}40^{s}$	149	?	
IKT 21	1E 0101.5-7226, HFPK 143, B0101-72.4, SNR J0103.2-7209	$01^h03^m13^s$	$-72^{d}08^{m}59^{s}$	62	CC	[6]
HFPK 334	SNR J0103.5-7247	$01^h03^m30^s$	$-72^{d}47^{m}20^{s}$	86	?	
1E 0102.2–7219	DEM S124, IKT 22, 1E 0102–72.3, HFPK 107, SNR 0102–72.3, SNR J0104.0–7202, B0102–7219	01 ^h 04 ^m 02 ^s	$-72^{d}01^{m}48^{s}$	44	CC	[10, 11, 12]
IKT 23	1E 0103.3-7240, DEM S125, HFPK 217, SNR 0103–72.6, SNR J0105.1–7223	01 ^h 05 ^m 04 ^s	$-72^{d}22^{m}56^{s}$	170	CC	[13, 14]
DEM S128	SNR 0103–72.4, B0104–72.2, ITK 24, HFPK 145, SNR J0105.4–7209	$01^{h}05^{m}23^{s}$	$-72^{d}09^{m}26^{s}$	124	Ia	[1, 2]
DEM S130	SNR J0105.6-7204	$01^h05^m39^s$	$-72^{d}03^{m}41^{s}$	79	?	
IKT 25	B0104-72.3, HFPK125, SNR 0104-72.3, SNR J0106.2-7205	$01^{h}06^{m}14^{s}$	$-72^{d}05^{m}18^{s}$	110	Ia/CC	[1, 2, 15–19]
N83C	NS83, SNR J0114.0–7317,DEM S147, SNR J011333–731704, B0113 = -729, SMC B0112–7333	$01^{h}14^{m}00^{s}$	$-73^{d}17^{m}08^{s}$	17	?	•

Note. Here we have listed the SNRs in order of R.A. Table adapted from Badenes et al. (2010) and Temim et al. (2015).

References. [1] van der Heyden et al. (2004); [2] Roper et al. (2015); [3] K. Auchettl et al. (2019, in preparation); [4] Hendrick et al. (2005); [5] Schenck et al. (2014); [6] Haberl et al. (2012a); [7] Owen et al. (2011); [8] Maitra et al. (2015); [9] Yokogawa et al. (2002); [10] Blair et al. (1989); [11] Blair et al. (2000); [12] Vogt & Dopita (2010); [13] Park et al. (2003); [14] Park et al. (2002); [15] Lee et al. (2011); [16] Lopez et al. (2014a); [17] Payne et al. (2007); [18] Hughes & Smith (1994); [19] Takeuchi et al. (2016).

 \sim 6 million stars from the Magellanic Clouds Photometric Survey (Zaritsky et al. 2002), Harris & Zaritsky (2004) derived color–magnitude diagrams in a rectilinear grid of 351 subcells that cover the central $4^{\circ} \times 4^{\circ}.5$ of the SMC. Each subregion is \sim 12′ \times 12′ in size, which corresponds to approximately 200 pc \times 200 pc in size at the distance of the SMC. In each of these subregions, the local SFH was derived using the SFH reconstruction program StarFISH (Harris & Zaritsky 2001). The SFH in each subregion was calculated for a look-back time from 4 Myr to 10 Gyr and was broken into three metallicity bins: $Z=0.001,\ 0.004,\$ and 0.008 (or [Fe/H] $=-1.3,\ -0.7,\$ and -0.4).

In Figure 2 (right panels), we plot the total SFR of the SMC as a function of look-back time over two different time ranges. The black solid line corresponds to the total SFH, and the dashed gray lines indicate the uncertainty in the total SFH. The pink, blue, and green curves indicate the SFR expected for the SMC assuming different metallicities ($Z=0.008,\ 0.004,\$ and 0.001, respectively). As discussed in detail in Sections 2 and 3 of Harris & Zaritsky (2004), the uncertainties in the SFR are most likely dominated by crowding effects. We note that studies of populations of B- and O-type stars found within the SMC (e.g., Korn et al. 2000; Bouret et al. 2013) have shown that Z=0.004 is representative of the stellar populations of the SMC. To be consistent with previous studies (such

as Badenes et al. 2009), we present all metallicities derived by Harris & Zaritsky (2001). To avoid the effect of metallicity on our results, we use the total SFR to characterize the SFHs associated with our sources.

The SMC has a complex SFH, which most likely results from the fact that the SMC is gravitationally bound with the LMC and Milky Way (e.g., Bekki et al. 2004; Bekki & Chiba 2005; Piatti et al. 2005; D'Onghia & Fox 2016). It is thought that the LMC and SMC underwent a recent and close encounter based on the detection of the Magellanic Bridge (Besla et al. 2012), proper-motion measurements of the LMC and SMC (Kallivayalil et al. 2013), and the distribution of the OB stars in the Magellanic Clouds and the Magellanic Bridge (Casetti-Dinescu et al. 2014). As the SMC and LMC formed a binary pair approximately 2 Gyr ago (Diaz & Bekki 2011), it is thought that this interaction triggered the enhanced SF seen at look-back times $\gtrsim 2 \,\mathrm{Gyr}$, as well as one more recently \sim 500 Myr ago. However, further studies are needed to confirm that these close encounters are the origin of these burst epochs (D'Onghia & Fox 2016).

Based on the SFH derived by Harris & Zaritsky (2004), for look-back times ≥8 Gyr ago, the SMC underwent significant SF, in which approximately 50% of all stars in the SMC were formed. Between 3 and 8.4 Gyr ago, the SMC underwent a period of quiescence, in which few stars were formed

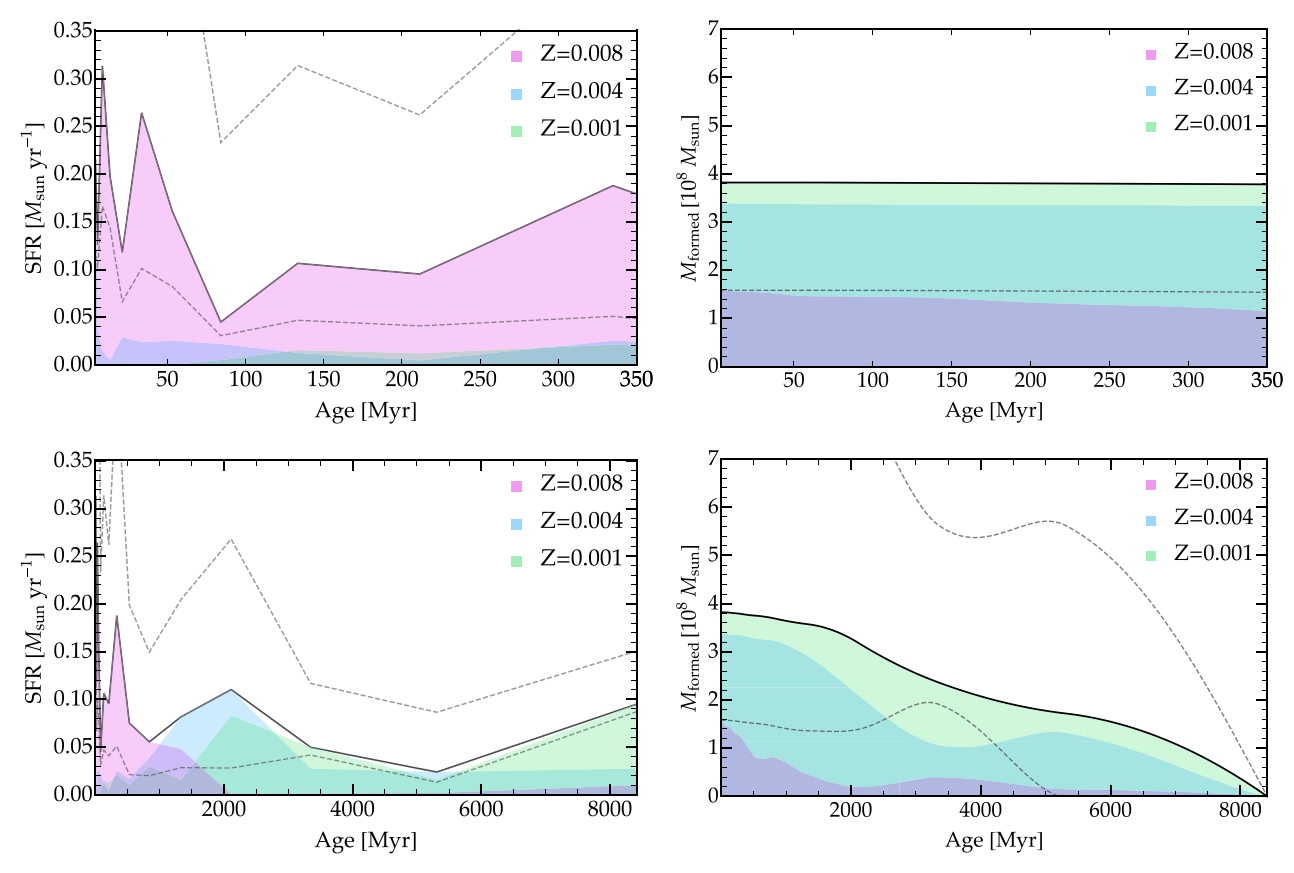


Figure 2. Left panels: total SFR of the SMC as a function of look-back time as seen in the three metallicity bins defined in Harris & Zaritsky (2004). The solid black line represents the total SFR, while the dashed gray lines represent the uncertainty on the total SFR. Right panels: cumulative stellar mass formed in the SMC as a function of look-back time as derived from integrating the SFR in each metallicity bin. We plot both the SFR and the cumulative stellar mass formed in the SMC over the timescales relevant for our analysis (top panels) and over the full look-back time of the SMC (bottom panels) for comparison.

compared to other periods during its SFH. More recently (<3 Gyr), the SMC has been actively producing stars at a rate of \sim 0.1 M_{\odot} yr⁻¹, with bursts of SF around 2.5 Gyr, 400 Myr, and 60 Myr ago.

Figure 2 (left panels) also highlights the evolution of the SMC's chemical enrichment. For a look-back time of $\gtrsim 3-5$ Gyr ago, the SMC exhibited little SF and thus very little variation in its metallicity during this early period (e.g., Dopita 1991; Da Costa & Hatzidimitriou 1998; Pagel & Tautvaišienė 1999; Piatti et al. 2001). However, when the SMC experienced two periods of enhanced SF at $\sim 1-3$ and $\sim 5-8$ Gyr ago, the mean metallicity of the SMC increased from [Fe/H] ~ -1.3 to a metallicity close to that of the present day ([Fe/H] ~ -0.6 ; Pagel & Tautvaišienė 1999; Dolphin et al. 2001; Piatti et al. 2001).

This relatively uniform increase in metallicity is likely responsible for the fact that the SMC does not exhibit the "abundance or age" gap observed for its star clusters, as seen for those in the LMC (e.g., Olszewski et al. 1991). As a consequence, the more metal-rich stars detected in the SMC are also the youngest, whereas the metal-poor stars are older and were formed $\gtrsim a$ few Gyr ago. This behavior is also seen in Figure 2 (right panels), where we have plotted the cumulative stellar mass formed in the SMC as a function of look-back time. Here, most of the metal-poor stars have an age $\gtrsim 0.5-1$ Gyr, and the more metal-rich stars tend to be $\lesssim 10-100\,\mathrm{Myr}$.

4. Source Selection and the Connection between SNRs and Their SN Explosions

4.1. Source Selection

We characterize the SFHs at the sites of all SNRs in the SMC, regardless of age, because a large number of these sources have not been typed before. Given that SNRs arise from explosions that occurred ~thousands of years ago, it can be difficult to discriminate the class of SN that led to each SNR. Typically, SNRs are typed based on their metal abundances measured using X-ray spectra (e.g., Vink 2012), by detecting a compact object associated with the source, or through their X-ray morphologies (Lopez et al. 2009a, 2009b, 2011; González-Casanova et al. 2014). Badenes et al. (2009) aimed to minimize the chances of misidentifying the LMC SNR progenitors by limiting their sample to only the youngest (and smallest) SNRs and those with well-determined SN types in the literature. Thus, they considered eight out of the 59 known SNRs in the LMC. By contrast, we examine the full population of SNRs in the SMC. In doing so, we aim to confirm the nature of the well-studied or controversial SNRs in the SMC, as well as to set initial constraints on those without any SN classification in the literature.

4.2. Progenitors of CC and Type Ia SNe

To characterize the progenitor masses of CC SNe, we adopted the single-star models of Zapartas et al. (2017). While

these models are based on rapid stellar evolution algorithms, they provide similar results to detailed stellar models from Eldridge & Tout (2004) and Eldridge et al. (2008) that were used in Badenes et al. (2009). Theoretically, these models predict that Type IIP SNe arise from 8–30 M_{\odot} red supergiants with their full H envelopes intact, Type IIb SNe come from 30–40 M_{\odot} red supergiants with partial H envelopes, and Type Ib/Ic result from stars >40 M_{\odot} that lose all of their H envelopes. The start is 10 models, the lifetime of an 8 M_{\odot} start is 10 models where M_{\odot} is 11 these models, the lifetime of an 8 M_{\odot} start is 12 models where M_{\odot} is 13 models where M_{\odot} is 14 models where M_{\odot} is 15 models where $M_{$

Observationally, the subtype of an SN is determined by early-time spectra of these events. However, characterizing SN progenitor masses is difficult, as it relies on the existence of pre-explosion images, and only a handful of sources have been observed prior to the SNe. Smartt et al. (2009) analyzed pre-SN explosion images and showed that known Type IIP/IIb SNe have progenitor masses of 8.5–16.5 M_{\odot} , suggesting a lack of high-mass red supergiant progenitors above 17 M_{\odot} . It is possible that this result arises from systematics related to underestimating progenitor masses due to extinction, or that stars $>17 M_{\odot}$ are produced by other SN types, such as Type IIL/IIn/IIb. However, Smartt et al. (2009) suggested that neither of these explanations is ideal, and thus it is likely that more massive progenitors possibly formed black holes with faint or nonexistent SNe. This conclusion was also reached by Eldridge et al. (2013), who attempted to place constraints on the progenitor masses of Type Ib/Ic SNe using the low ejecta masses derived from the literature (see review by Smartt 2015) and upper limits from pre-explosion images. These authors noted that the rates of Type Ib/Ic SNe are quite high and can only be achieved if Type Ib/Ic SNe result from a mixed population of single stars and binary systems with stars of initial mass $<20\,M_{\odot}$.

Generally, it is difficult to distinguish the CC SN subtype of SNRs. Only a handful of SNRs have well-constrained CC SN subtypes derived using X-ray, infrared, or optical observations. Due to the challenges of subtyping SNRs, our study aims to ascertain whether individual SNRs likely arose from a CC explosion, based on a recent burst of SF, and the probable progenitor mass using the massive star lifetimes of Zapartas et al. (2017), rather than focusing on what subtype of explosion it underwent.

It has been shown that massive O stars are found in binary systems. Of these, more than 70% will have their evolution affected by binary interaction, with approximately one-third of these massive stars being the result of a binary merger (Sana et al. 2012). Recently, Zapartas et al. (2017) demonstrated that $\sim\!15\%$ of the massive stars found in these binary systems will undergo a delayed CC SN, exploding after $\sim\!50\text{--}200\,\mathrm{Myr}$, in contrast to the $\sim\!3\text{--}50\,\mathrm{Myr}$ expected for a single massive star. Consequently, SF at these look-back times may suggest a CC

found in a binary system.

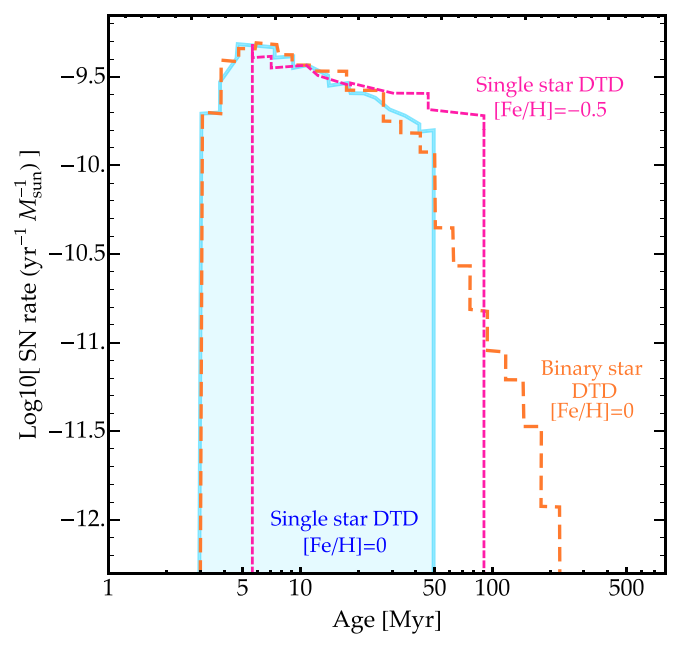


Figure 3. Effect of binarity (orange dashed curve) and rapid rotation (magenta dotted curve) on the DTD of CC SNe arising from a single-star population (blue shaded region). Here the solar metallicity ([Fe/H] = 0) single- and binary-star DTDs are adapted from Zapartas et al. (2017), while we use the MESA isochrone and stellar track of Choi et al. (2016), which assumes that all stars rapidly rotate, to quantify the effect that rapid rotation in a low-metallicity environment ([Fe/H] = -0.5) has on the lifetimes, and thus the DTD, assuming a single-star population.

SN of a close binary system or a "prompt" Type Ia SN origin, which is discussed below.

A natural consequence of binary interaction is that at least \sim 20% of massive main-sequence stars will be rapidly rotating (e.g., de Mink et al. 2013). Rapid rotation increases mixing within stars, extending the lifetimes and evolution of those stars (Maeder & Meynet 2000). In low-metallicity environments, the winds of massive main-sequence stars are weak (e.g., Vink et al. 2001; Mokiem et al. 2007). As stars lose their angular momentum via stellar winds (Langer 1998), stars in these environments will lose less angular momentum and thus spin much faster than those found in solar-metallicity environments (e.g., Martayan et al. 2007; D'Antona et al. 2015; Milone et al. 2016; Bastian et al. 2017; Dupree et al. 2017). In fact, Hunter et al. (2008, 2009) measured the rotational velocities of a large population of massive stars in both the Milky Way and Magellanic Clouds and found that massive stars in the SMC rotate faster than those in the Milky Way with a 3σ confidence.

In Figure 3, we plot how binarity ¹⁰ and rapid rotation alter the delay-time distribution (DTD) of CC SNe arising from a single-star population. Plotted as the blue shaded region and orange dashed curve are the solar metallicity ([Fe/H] = 0) single-star and binary-star DTD, respectively, from Zapartas et al. (2017). One can see that binarity leads to a fraction of progenitors that will undergo CC well after all massive single stars have already exploded.

To illustrate the effect that rapid rotation can have on the lifetimes of massive single-star populations, we use the MESA isochrone and stellar tracks of Choi et al. (2016), which assumes that all stars are rapidly rotating. Using the same form

⁷ We note that Type Ib/Ic SNe can be bipolar/jet-driven. In fact, as rapid rotation without extensive mass loss is required to produce bipolar SNe, it is expected that these explosions will be found predominantly in low-metallicity environments like the SMC (e.g., Ramirez-Ruiz et al. 2002; Izzard et al. 2004).
8 The discovery of Type Ib SN iPTF13bvn by Cao et al. (2013) has brought into question whether Type Ib SNe result predominantly from progenitors >40 M_{\odot} . Work by, e.g., Bersten et al. (2014) and Eldridge et al. (2015) has shown that this explosion likely arose from a low-mass progenitor (~11 M_{\odot})

For example, Cassiopeia A is thought to have been from a Type IIb explosion based on the expansion properties of its shock front (Chevalier & Oishi 2003; Chevalier 2005) and light echo spectra (Krause et al. 2008). See review by Milisavljevic & Fesen (2017) for a more detailed overview.

 $[\]overline{^{10}}$ Here and throughout the text, we define binarity as the effect of binary interactions on a stellar population.

of the DTD as for a single-star population at solar metallicity, we have plotted the corresponding DTD (the magenta dotted curve in Figure 3), assuming a metallicity similar to that of the SMC ([Fe/H] = -0.5). One can see that the lifetime for the last SN assuming a single-star population can be significantly delayed in the rapidly rotating, low-metallicity case. However, we note that not all massive stars in the SMC are rapidly rotating (Hunter et al. 2008, 2009); thus, the extent of this delay is likely an upper limit for when the last CC SN would explode.

As the SMC is a low-metallicity galaxy, we also note the effect that metallicity, independent of rotation, has on the lifetimes of SNe. Recently, using their suite of binary stellar evolution models that span a wide range of masses and metallicities, Eldridge et al. (2017) investigated the effect that metallicity alone has on the DTDs of single- and binary-star populations. They found that the effect of metallicity on the age distribution of SNe arising from a single-star population is relatively minor, while for binary populations, there is a small increase in the lifetimes (see Figure 19 of Eldridge et al. 2017).

For Type Ia SNe, the identity of their progenitors and the mechanism responsible for their explosion remain uncertain both theoretically and observationally (see, e.g., Maoz et al. 2014; Maeda & Terada 2016). These events are thought to occur when either the mass accreted onto the WD comes close to the Chandrasekhar limit (e.g., Hachisu et al. 1996; Han & Podsiadlowski 2004) or the objects merge or collide on the dynamical timescales of these systems (e.g., Iben & Tutukov 1984; Guillochon et al. 2010; Sim et al. 2010; van Kerkwijk et al. 2010; Dan et al. 2011).

Significant work, both observationally and theoretically, has been done to explore the single- and double-degenerate scenarios of Type Ia explosions (see the review by Maoz et al. 2014 and more recent work by, e.g., Yamaguchi et al. 2015 and Martínez-Rodríguez et al. 2016). In terms of SFHs, Type Ia SNe have been shown to be associated with galaxies that exhibit a variety of SFHs and galaxy properties (e.g., Aubourg et al. 2008; Maoz & Badenes 2010; Li et al. 2011; Maoz & Graur 2017).

As a consequence, Type Ia SNe arise from a wide range of progenitors of various ages, with the rate of Type Ia SNe detected well described using a simple power law (also called the DTD; see Section 5 for more details). As such, the young ("prompt") progenitor population that produces Type Ia SNe on timescales of $\lesssim 100$ –330 Myr (e.g., Aubourg et al. 2008; Maoz & Badenes 2010 and references therein) has a much greater representation than the older ("delayed") progenitor population that explodes on timescales of \sim Gyr and are not associated with SF.

5. Local SFH Around Individual SNRs

In disk-dominated galaxies, the mixing of stellar populations due to radial migration from the gravitational interaction of stellar populations results in the SFHs directly surrounding an SNR to be representative of the SN progenitor up to a specific look-back time (e.g., Sellwood & Binney 2002; Roškar et al. 2012; Di Matteo et al. 2013). However, for dwarf galaxies, which lack a well-defined disk, bar, or spiral arm, simulations have shown that stellar mixing and migration only become important (if at all) on cosmological timescales (e.g., El-Badry et al. 2016 and references therein). As a consequence, the stellar populations associated with these galaxies change very little over the lifetime of the host galaxy

(e.g., Stinson et al. 2009; Schroyen et al. 2013). The SMC, which is an irregular dwarf galaxy, does not exhibit a well-defined disk or spiral structure (e.g., Stanimirović et al. 2004). As a result, stellar mixing and migration is likely not an important effect in the SMC, and thus the stellar populations surrounding each of the SNRs should be representative of the SN progenitors. For CC SNe, this conclusion is also supported by work done by Anderson & James (2008), who showed that the overall population of CC SNe closely follows $H\alpha$ emission, an excellent tracer of recent SF, with SNe that result from high-mass progenitors (such as SNe Ib/c) in regions of strong $H\alpha$ emission (see Figure 1).

Additionally, even though most massive stars are born in a binary system, a majority of these systems are disrupted after one of the companions undergoes CC. Then these unbounded, young massive stars can gain kick velocities of a few km s⁻¹, becoming what is known as walkway stars (de Mink et al. 2012), while a small fraction of these companions become runaway stars with velocities >30 km s⁻¹ (Eldridge et al. 2011; Renzo et al. 2018). For stars $>15\,M_{\odot}$, $\sim10\%$ will have velocities consistent with a walkaway star, while $\sim0.5\%$ will have velocities >30 km s⁻¹ (Renzo et al. 2018).

In low-metallicity environments like the SMC, runaway stars tend to be more common, as they experience less mass loss; thus, they are found in systems that are more difficult to disrupt without strong kicks. Renzo et al. (2018) showed that both walkaway and runaway stars with masses $>7.5\,M_\odot$ travel a mean distance of $\sim\!163\,\mathrm{pc}$ in a low-metallicity environment before exploding as SNe, and more massive progenitors travel substantially less (Eldridge et al. 2011; Renzo et al. 2018). Since the size of the subregions used in our analysis is $\sim\!200\,\mathrm{pc}$, only the fastest runaway stars would drift significantly from their birthplace. However, as these very fast objects are rare, it is unlikely that they contribute significantly to the SFH measured in the proximity of each SNR. As such, the stellar populations surrounding each remnant should be representative of the SN progenitors.

In Figure 4, we plot the local SFHs as a function of lookback time for each SNR in the SMC using the subcell that is coincident with each SNR. We have overlaid a dashed vertical line to denote the lifetime of an isolated 8 M_{\odot} star assuming solar metallicity (Zapartas et al. 2017). Here we focus on the most recent time bins that are relevant for progenitor identification. Figure 5 shows the same SFHs for each SNR as in Figure 4, but we have binned the SFH into three time intervals corresponding to the progenitor mass ranges of 8–12.5, 12.5–21.5, and >21.5 M_{\odot} . Additionally, we have included the 50-200 Myr time bin to aid in identification of massive progenitors that may have undergone delayed CC due to binary interaction and rapid rotation (e.g., de Mink et al. 2013; Schneider et al. 2015; Zapartas et al. 2017) or the low metallicity (e.g., Pols et al. 1998) of the SMC. Overlaid at the top of each plot in Figure 5 is the time when stars of a given zero-age main-sequence (ZAMS) mass M_{ZAMS} would have formed, assuming the single-star models of Zapartas et al.

To make statistical statements in regard to the progenitor distributions implied by the local SFHs near SNRs, we take advantage of current DTDs associated with both CC and Type Ia SNe. The DTD is an important tool used in stellar population studies, as it encapsulates the timescales in which members of a particular stellar population born in a burst of SF will go

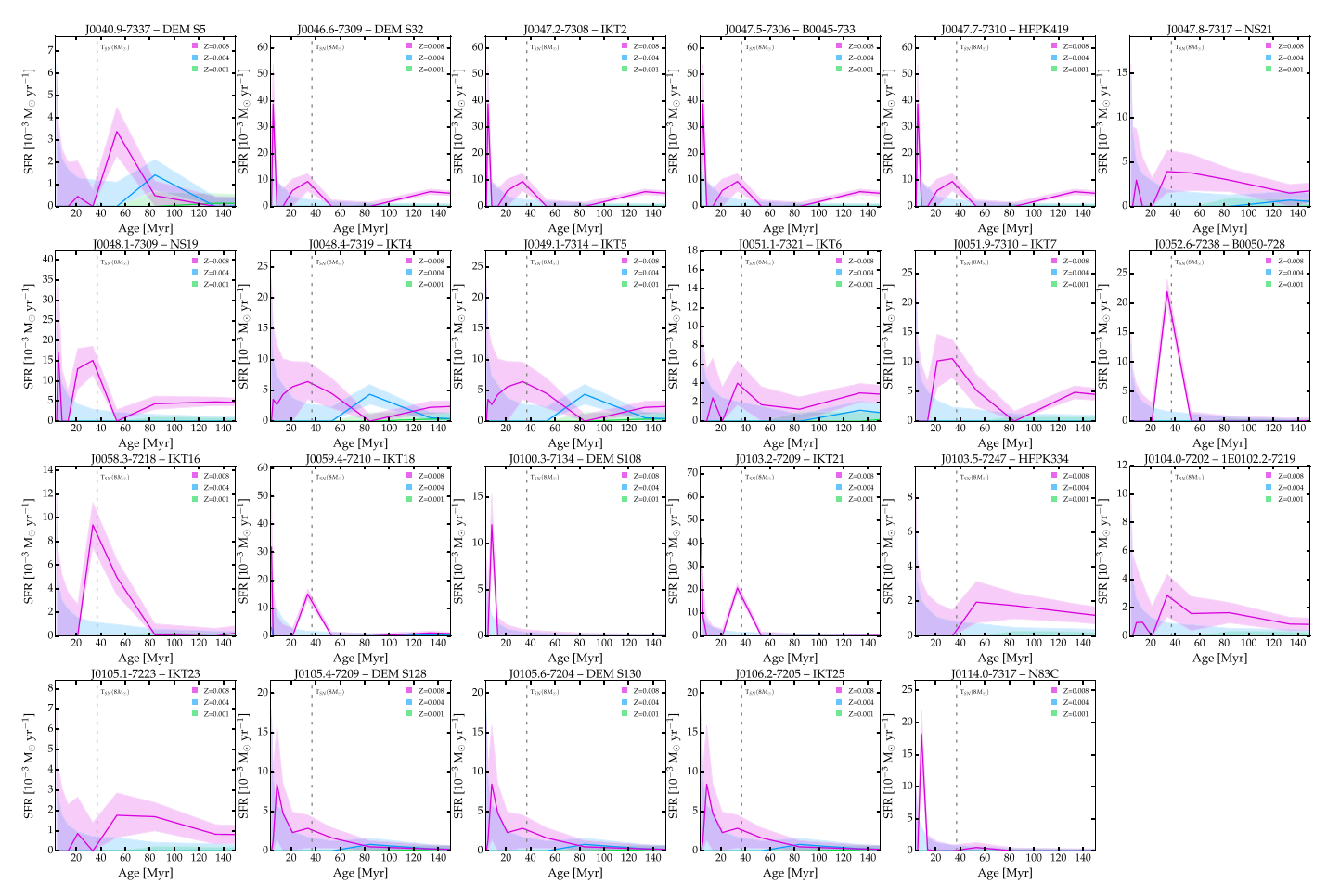


Figure 4. Local SFHs of the SMC SNRs as a function of look-back time up to 150 Myr in three metallicity bins. The colored, shaded bands correspond to the 1σ uncertainty in the SFR as determined by Harris & Zaritsky (2004). The dashed vertical line is the lifetime of an isolated $8 M_{\odot}$ star from the models of Zapartas et al. (2017).

undergo an SN (e.g., Maoz & Mannucci 2012; Maoz et al. 2014). Combined with the local SFH, the DTD allows us to constrain the progenitor origin of each SNR, since the form of the DTD is set by the progenitor population and the stellar and binary evolution of that population (e.g., Maoz & Mannucci 2012; Maoz et al. 2014; Maoz & Graur 2017; Zapartas et al. 2017).

As Type Ia SNe originate from lower-mass systems than CC SNe, the former tend to have delay times on the order of Myr to Gyr. As such, most studies related to observationally constraining the DTDs of SNe have focused on quantifying the Type Ia DTD using extragalactic SN surveys (see review by Maoz et al. 2014). However, CC SNe (which arise from more massive progenitor systems) have delay times that are significantly shorter, on timescales of Myr. Consequently, it is much more difficult to observationally constrain these timescales following the same techniques used for Type Ia SNe (e.g., Maoz & Badenes 2010; Maoz et al. 2011), since the DTD of CC SNe requires a much more accurate determination of the ages of the underlying stellar population to derive this distribution.

Significant theoretical effort has gone into determining the DTD of CC SNe. Zapartas et al. (2017) performed a detailed population synthesis study to derive the DTD of CC SNe, taking into account that 70% of massive stars evolve in binary systems (e.g., Sana et al. 2012 and references therein).

Compared to the DTD of CC SNe assuming a single-star population that cuts off after the last single star explodes ($\sim 50\,\mathrm{Myr}$), Zapartas et al. (2017) found that binarity tends to extend the DTD to longer delay times (50–200 Myr). These delayed events represent a nonnegligible contribution ($\sim 15.5\%$) to the total number of CC SNe assuming a Kroupa initial mass function (IMF). In fact, the enhanced SN rate between 35 and 330 Myr seen in the LMC and SMC by Maoz & Badenes (2010) could suggest a substantial contribution of delayed CC SNe.

Due to the importance of using DTDs to guide our conclusions about the nature and progenitor properties of each SNR, we convolve our local SFHs (Figure 5) with recent DTDs for both Type Ia and CC SNe. For our study, we use the Type Ia DTD derived by Maoz & Graur (2017), which has the form of $t^{-(1.1\pm0.1)}$ and a total integrated rate of $N/M_{\star} = (1.3\pm0.1)\times10^{-3}\,M_{\odot}^{-1}$. For CC SNe, we use both the single-and binary-star population DTDs derived by Zapartas et al. (2017) to quantify the masses of the progenitors and test whether any of the SMC SNRs could have resulted from a delayed CC explosion.

By correlating the timing of the various SF bursts, we can estimate the mass of the progenitor and associate a likelihood that the SNR results from a particular SN subtype. To estimate the likelihood, we convolve the three most recent SFH bins that are less than 50 Myr with a standard Salpeter IMF

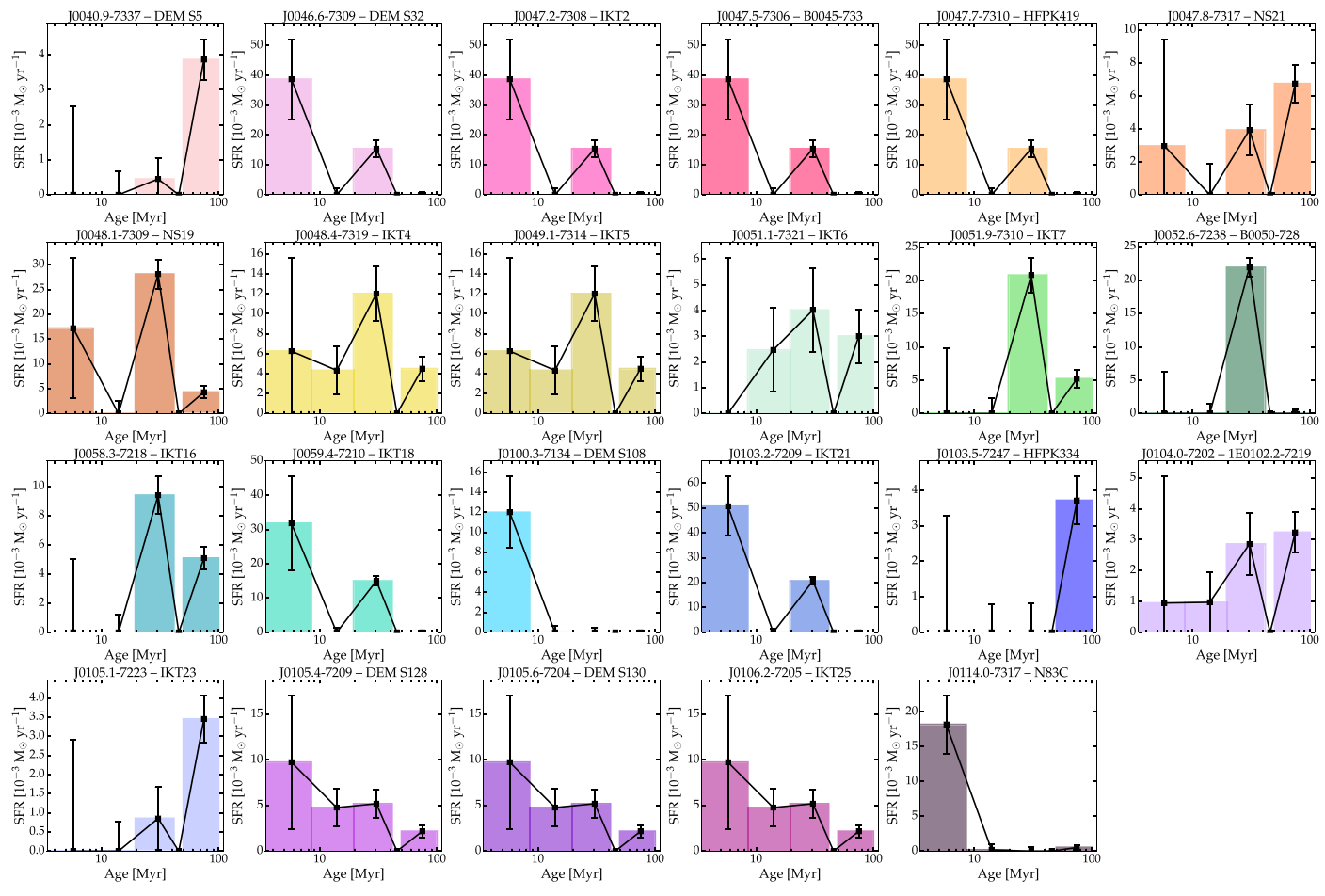


Figure 5. Recent SFHs in the vicinities of the SMC SNRs. Here we plot only the SFH associated with a metallicity of Z = 0.008, comparable to the measured metallicity of the SMC now. We have binned the SFHs into three mass intervals: 8-12.5, 12.5-21.5, and $>21.5 M_{\odot}$. We have also included the 50–200 Myr time range to identify possible delayed CC SNe due to either the low-metallicity environment or binary interaction. The ranges at the top of the panels correspond to the ZAMS progenitor masses for different ages, as derived from the single-star models of Zapartas et al. (2017).

(Salpeter 1955) to determine the likelihood that the progenitors in one of the three mass intervals result in a CC SNe.

For sources thought to arise from SNe Ia, we quantify the fraction of the stellar population that would result from the prompt and delayed channels by assuming that the rate of SNe Ia ($R_{\rm Ia}$) in a galaxy is given by $R_{\rm Ia} = R_{\rm delayed} + R_{\rm prompt}$. Here we assume that prompt and delayed SNe Ia arise on timescales of $\sim 100\,{\rm Myr}$ and $> 2.4\,{\rm Gyr}$, respectively (Maoz et al. 2012), and convolve the local SFR within these time frames with the Type Ia DTD of Maoz & Graur (2017).

Using the total SFR and cumulative stellar mass plots presented in Figure 2 (bottom panels), we can calculate R_{delayed} and R_{prompt} for the whole SMC: $R_{\text{delayed}} = 10\%$ and $R_{\text{prompt}} = 10\%$ 90%. This is quite different from what is derived for the LMC: $R_{\text{delayed}} = 41\%$ and $R_{\text{prompt}} = 59\%$ (Badenes et al. 2009). However, this is not so surprising, since the rate of SNe per year used by Badenes et al. (2009) is an order of magnitude lower than the SN Ia rate derived from recent observations (e.g., Maoz & Graur 2017). Using the SN Ia rate of Sullivan et al. (2006; which was adopted by Badenes et al. 2009 in their calculation), we find that $R_{\text{delayed}} = 33\%$ and $R_{\text{prompt}} = 67\%$, which is still lower than what is derived for the SMC. One possible reason for this disparity between the SMC and LMC is their different metallicities. In particular, it has been shown by Kistler et al. (2013) that the mass of a carbon-oxygen WD increases for lower metallicities. The stars that produce these more massive WDs would evolve much more rapidly compared to those found in high-metallicity environments, which could lead to the prompt channel dominating the SNe Ia in low-metallicity galaxies.

In the following subsections, we provide a general overview of the results we obtained by considering both the SFH around each SNR with the properties of the SNR and its environment derived from X-ray/optical observations. A more detailed description of these properties and SFHs of each of the SMC remnants can be found in Appendix A. Table 2 summarizes the possible progenitor type of each SNR based on the SFHs and the likelihood of a particular CC progenitor or prompt/delayed Type Ia progenitor.

5.1. CC SNRs

Of the 23 SNRs in the SMC, only five (HFPK 419 [SNR J0047.7–7310], IKT 6 [B0049–73.6], IKT 16 [SNR J0058.3–7218], 1E 0102.2–7219 [SNR B0102–7219], and IKT 23 [SNR 0103–72.6]) have been classified robustly as arising from a CC explosion. Five other remnants, DEM S32 [SNR J0046.6–7309], IKT 2 [B0045–73.4], IKT 7 [SNR J0051.9–7310], IKT 18 [SNR J0059.4–7210], and IKT 21 [B0101–72.4], have also been suggested to be CC SNRs in the literature, while IKT 5 [SNR 0047–73.5] and IKT 25 [SNR 0104–72.3] have been claimed as Type Ia or CC SNRs by

Table 2
SMC SNR Classification Based on SFH and the Likelihood of Their Progenitor Properties

	SN Origin Based on SFHs	Evidence of Delayed CC?	Assuming Single-star Population			Assuming Binary-star Population							
Name			$N_{\rm CC}/N_{\rm Ia}$	% of CC SNe Progenitors from		$N_{ m CC}/N_{ m Ia}$	% of CC SNe Progenitors from			% of Type Ia Progenitors from			
				$>$ 21.5 M_{\odot}	$12.521.5~M_{\odot}$	8–12.5 <i>M</i> _⊙		$>$ 21.5 M_{\odot}	$12.521.5M_{\odot}$	$812.5~M_{\odot}$	Delayed CC	Prompt	Delayed
DEM S5	CC _p	d	3	0	0	100	3	0	0	44	56	95	5
DEM S32	CC _p		14	92	0	8	15	93	0	7	0		
IKT 2	CC _p		14	92	0	8	15	93	0	7	0		
B0045-733	CC _p	•••	14	92	0	8	15	93	0	7	0		•••
HFPK 419	CC ^{a b}		14	92	0	8	15	93	0	7	0		
NS 21	CC _p	(d?)	3	78	0	22	3	75	0	19	6	99	1
NS 19	CC _p	(d?)	11	74	0	26	12	75	0	24	1		
IKT 4	CC	(d?)	7	59	17	24	7	58	18	22	2	98	2
IKT 5	CC _p	(d?)	7	59	17	24	7	58	18	22	2		
IKT 6	CC ^a	(d?)	4	0	54	46	4	0	53	39	8	99	1
IKT 7	CC	(d?)	6	0	0	100	7	0	0	93	7		
B0050-728	CC _p	•••	9	0	0	100	10	0	0	100	0		
IKT 16	CC ^a	(d?)	6	0	0	100	6	0	0	93	7		
IKT 18	CC _p		62	91	0	9	63	92	0	8	0		
DEM S108	CC _p	•••	17	100	0	0	17	100	0	0	0		
IKT 21	CC		139	92	0	8	141	93	0	7	0	87	13
HFPK 334	Ia	•••	3	0	0	0	3	0	0	0	100	96	4
1E 0102.2-7219	CC ^a	(d?)	5	49	20	31	5	47	20	27	6		
IKT 23	CC ^a	d	3	0	0	100	4	0	0	56	42		
DEM S128	CC _p	(d?)	25	76	15	9	26	75	16	8	1		
DEM S130	CC_p	(d?)	25	76	15	9	26	75	16	8	1		
IKT 25	CC ^a	(d?)	25	76	15	9	26	75	16	8	1		
N83C	CC _p	•••	32	100	0	0	32	99	0	0	1		

Notes. Here $N_{\rm CC}/N_{\rm Ia}$ represents the relative number of CC versus Type Ia progenitors and is derived using the Type Ia DTD of Maoz & Graur (2017) and the CC DTD assuming either a single or binary stellar population of Zapartas et al. (2017). In the third column, CC = based on its SFH and properties, this remnant arose from a CC SNe; Ia = based on its SFH and properties, this remnant likely arose from a Type Ia SNe; d = the SFH is strongest in the 50–100 Myr time bin, suggesting that this SNR may have resulted from a delayed CC explosion; (d?) = the SFH shows some SF in the 50–100 Myr bin, which may suggest a delayed CC explosion.

9

^a The SNR has independent evidence in support of SN classification derived from the SFH.

b Source associated with an H II region, dense environment, star-forming region, stellar cluster, or emission nebula.

different authors. Among these 12 SNRs, five have progenitor mass estimates in the literature, and we compare our results below to test the robustness of the SFHs as tools to estimate progenitor masses.

The most striking feature of the SFHs of the stellar populations associated with a majority of these SNRs is the strong burst of SF seen at times <50 Myr, similar to the CC LMC SNR sample presented in Badenes et al. (2009). However, some variation in the SFHs between sources is evident. For example, we find that for IKT 25, the SFR burst is less than that seen around, e.g., HFPK 419 and IKT 16. For IKT 6 and 1E 0102.2–7219, their associated stellar populations do not exhibit any bursts in SFR, instead showing persistent SF that increased 10–100 Myr ago.

In addition to their burst of SF <50 Myr ago, we also note that the stellar populations associated with IKT 6, IKT 16, 1E 0102.2–7219, IKT 23, IKT 7, IKT 5, and IKT 25 exhibit a strong peak of SF in the 50–200 Myr bin. This burst of SF suggests that some of the stellar population associated with these remnants may have undergone a delayed CC due to either binary interaction, rapid rotation, or low metallicity. Assuming a binary-star population DTD, it seems that for a majority of them, no more than \sim 10% of the stellar population underwent delayed CC. However, for IKT 23 and IKT 25, our analysis suggests that a significant fraction (\sim 42% and \sim 22%, respectively) of their stellar population underwent delayed CC.

For IKT 6, 1E 0102.2–7219, IKT 2, and IKT 25, which have independent progenitor mass estimates from detailed X-ray or optical studies, the SFRs of their stellar populations <50 Myr ago are consistent with the lifetimes of the progenitor masses implied from these studies. This suggests that for a majority of known CC remnants, the SFH can provide a relatively robust and independent confirmation of progenitor masses for these systems. The exception to this is IKT 23, whose SFR <50 Myr ago implies that 100% of the CC SN progenitors associated with this remnant have masses of 8–12.5 M_{\odot} , which is slightly below the ~18 M_{\odot} suggested by Park et al. (2003).

The stellar populations associated with IKT 16, IKT 2, 1E 0102.2–7219, and IKT 7 exhibit a strong burst of SF consistent with either an 8–12.5 or a >21.5 M_{\odot} progenitor. The progenitor masses implied by the SFHs associated with these remnants are consistent with theoretical work by, e.g., Sukhbold et al. (2016), who suggested that neutron stars are produced in SNe of stars <30 M_{\odot} . These four remnants have been suggested to either harbor a pulsar wind nebula (PWN)/central compact object or be associated with a Be/X-ray pulsar system (Yokogawa et al. 2000; Williams et al. 2006; Owen et al. 2011; Haberl et al. 2012a; Maitra et al. 2015; Vogt et al. 2018).

The stellar populations associated with the three oxygen-rich remnants, IKT 6, 1E 0102.2–7219, and IKT 23, have some similarities in their SFH <50 Myr ago. Our method is unable to constrain whether the oxygen-rich SNRs are associated with a particular progenitor mass. We should note that all three show significant SF between 50 and 200 Myr ago; however, there are also a number of other remnants that are not oxygen-rich and do show this burst at much later times.

Out of the 12 CC SNRs discussed above, eight of them (HFP 419, 1E 0102.2–7219, DEMS 32, IKT 2, IKT 18, IKT 21, IKT 5, and IKT 25) have SFHs that suggest that a large fraction of CC SN progenitors associated with the stellar population of

each remnant have a mass $>21.5\,M_{\odot}$. The other four remnants (IKT 6, IKT 16, IKT 23, and IKT 7) have SFHs consistent with a progenitor $<21.5\,M_{\odot}$. This result will be discussed further in Section 6.

5.2. Possible Type Ia SNRs

Four out of the 23 SMC SNRs have been suggested to arise from SNe Ia. These include IKT 5 [SNR 0047–73.5], IKT 25 [SNR 0104–72.3], IKT 4 [SNR J0048.4–7319], and DEM S128 [SNR 0103–72.4]. As discussed in the previous section, IKT 5 and IKT 25 have SFHs and properties that are more consistent with CC SNRs than Type Ia SNRs. Thus, we focus on IKT 4 and DEM S128 in this section.

The SNe Ia occur in a wide range of environments, with little to intense SF of both metal-poor and metal-rich populations (James & Anderson 2006; Badenes et al. 2009; Wang et al. 2013; Galbany et al. 2014; Anderson et al. 2015). To date, no SMC SNRs have confirmed classifications as Type Ia events based on, e.g., X-ray metal abundances or light echoes. Thus, our SFH analysis provides preliminary constraints on the nature of possible Type Ia SNRs in the SMC.

It was suggested that IKT 4 was a Type Ia SNR based on the detection of enhanced Fe from a shallow *XMM-Newton* observation (van der Heyden et al. 2004). The SF associated with IKT 4 exhibits an extended peak of intense metal-rich SF < 50 Myr ago and a smaller peak of metal-poor SF ~90 Myr ago. Assuming that this remnant is from a Type Ia event, the probability that this source arose from a prompt progenitor is 98%. This conclusion is similar to that found by Badenes et al. (2009), who showed that N103B (an SNR in an actively star-forming region in the LMC) likely arose from a young, prompt Type Ia progenitor.

The proximity of IKT 4 to the star-forming region N19 suggests that it is possible that IKT 4 arose from a CC explosion rather than a Type Ia SN. The X-ray data of this source are not sufficiently deep to constrain its abundance properties, and thus the nature remains uncertain. If this remnant results from a CC of a massive star, our estimates from the SFH of this source indicate that 24%, 17%, and 59% of the CC progenitors have a mass of 8–12.5, 12.5–21.5, or $>21.5 M_{\odot}$, respectively.

It was suggested that DEM S128 arose from a Type Ia SN based on center-filled X-ray emission that exhibited enhanced Fe abundances (van der Heyden et al. 2004; Roper et al. 2015). However, the SFH of the stellar population associated with DEM S128 shows intense, metal-rich SF that peaked \sim 10 Myr ago, consistent with the SFH from a CC progenitor. Given that DEM S128 is associated with an H II region with the same name (Bica & Schmitt 1995), as well as its recent, active SF, we believe that DEM S128 more likely resulted from a CC explosion than a Type Ia event. Based on our estimates, 76% of CC progenitors in the region are >21.5 M_{\odot} stars, and 9% (15%) are from 8–12.5 M_{\odot} (12.5–21.5 M_{\odot}) stars, respectively.

5.3. Previously Unclassified SNRs

For nine out of the 23 SNRs in the SMC, their explosive origin is unknown or not well constrained. This includes DEM S5 [SNR J0040.9–7337], B0045–733 [SNR J0047.5–7306], NS 21 [SNR J0047.8–7317], NS 19 [SNR J0048.1–7309], B0050–728 [SNR J0052.6–7238], DEM S108 [SNR J0100.3–7134], HFPK 334 [SNR J0103.5–7247], DEM S130 [SNR J0105.6–7204], and

N83C [SNR J0114.0–7317]. The main reason for their lack of classification comes from either the faintness of the source itself or the shallow observations overlapping these sources. As such, combined with what information is available about each source, the SFHs of the stellar populations associated with these remnants can help us better constrain the possible SN origin.

All nine remnants exhibit weak, thermal X-ray emission, making it difficult to constrain the presence of enhanced abundances that can help constrain the nature of the SNe. However, optical observations of DEM S5 detect bright [O III] emission associated with its shell, which may suggest that this remnant is an oxygen-rich CC SNR, much like 1E 0102.2–7219 and IKT 23, which also show bright [O III] (Payne et al. 2007). However, some Type Ia SNRs (e.g., *Kepler*, Blair et al. 2007; Reynolds et al. 2007; Burkey et al. 2013; N103B, Williams et al. 2014b) also exhibit strong [O III] emission and are found to be interacting with dense circumstellar material.

All of these previously unclassified remnants, except for HFPK 334, are surrounded by stellar populations that exhibit strong SF <50 Myr ago. Their SFHs have well-defined bursts of various intensities, consistent with that seen surrounding CC SNe. As nearly all of these remnants are found to be either interacting with dense material, like DEM S5 and N83C (Filipović et al. 2008; Temim et al. 2015), or close to a starforming region/cluster (e.g., B0045-733, NS 19, B0050-728, and N83C) or H II regions (e.g., NS 21, B0050-728, and DEM S130), it is likely that these remnants arise from the CC of massive stars. Under this assumption, the majority of the CC SN progenitors associated with these SNRs have a mass $>21.5 M_{\odot}$. Of these, DEM S5, NS 21, NS 19, DEM S130, and N83C exhibit varying degrees of SF \sim 50–200 Myr ago, which may imply that a fraction of the stellar population underwent delayed CC. However, this fraction is no more than \sim 5% for most of these sources. By contrast, the SF of DEM S5 is dominated by significant SF \sim 50-200 Myr ago, implying that \sim 56% of the progenitors associated with this remnant underwent delayed CC.

Compared to all other SNRs in the SMC, the SFH of HFPK 334 is quite unique. Crawford et al. (2014) showed that HFPK 334 is expanding into a low-density environment, a characteristic commonly associated with Type Ia SNRs, such as SN1006 (Koyama et al. 1995), RX J1713.7–3946 (Koyama et al. 1997; Slane et al. 1999), and SNR 0509–67.5 (Warren & Hughes 2004). It is the only SNR with virtually no SF in the last ~50 Myr (although the uncertainties are large for the last ~5 Myr). The peak SF of HFPK 334 occurred 50–1000 Myr ago, similar to the SFH observed for the Type Ia SNR N103B in the LMC (Badenes et al. 2009). If HFPK 334 is the result of a CC explosion, then the lack of SF since 50 Myr ago indicates a delayed explosion due to rapid rotation or binary interaction. However, we are unable to use its SFH to place constraints on the possible mass of its progenitor, assuming it arose from a CC SN.

Given its low-density environment and unique SFH, we suggest that HFPK 334 likely arose from an SN Ia. Under this assumption, the SF between 64 and 180 Myr ago suggests that it arose from a prompt Type Ia progenitor with a probability of 96%. As such, unlike LMC SNR N103B, which showed a strong peak of emission at \sim 12 Myr, suggesting that this source may have resulted from a young (<150 Myr) progenitor, it is

likely that HFPK 334 arose from an older (>150 Myr), Z = 0.004-0.008 progenitor that underwent a prompt Type Ia explosion. As this remnant is expected to be relatively evolved (with an age of >1.4 kyr), the X-ray spectrum is thought to be dominated by emission with interstellar medium (ISM) abundances (Crawford et al. 2014). Deeper observations would be required to confirm the nature of this source and determine whether its properties are consistent with those of Type Ia SN explosion models (e.g., Badenes et al. 2008).

6. Discussion

We have examined the stellar populations in the vicinities of 23 known SNRs in the SMC. Using the SFH maps of Harris & Zaritsky (2004) and recent Type Ia and CC DTDs, we have attempted to characterize the nature of the progenitors of each SNR based on when the SFR peaked. We have compared our findings to the SNR properties, such as metal abundances, X-ray morphologies, and surrounding environments. Despite the limitations of constraining the progenitors using the SFHs, we have found that the explosive origins ascertained from the SNR properties are generally consistent with those predicted from the proximal stellar populations. In particular, sources classified as CC SNRs from detailed spectral modeling and abundance estimates from deep X-ray studies had the best agreement with the SFH results (e.g., 1E0102.2-7219, Blair et al. 2000; IKT 2, Yokogawa et al. 2002; IKT 23, Park et al. 2003; IKT 25, Lopez et al. 2014a).

6.1. Comparison with Independent Progenitor Mass Estimates

From our study, the vast majority of the stellar populations associated with the SNRs in the SMC have SFHs consistent with CC origins. Based on our DTD convolved local SFHs, we estimate the possible masses of the CC progenitors. In Figure 6, we have plotted the progenitor mass distribution of the known CC SNRs listed in Section 5.1 (left panel) and all SNRs classified as CC in our analysis (right panel). Here the area of the plot marker represents the likelihood that each source arose from a progenitor of mass 8–12.5, 12.5–21.5, or >21.5 M_{\odot} , assuming a binary-star population. We find that most of the CC SMC SNRs have SFHs that are consistent with a progenitor mass of 8–12.5 or >21.5 M_{\odot} .

For IKT 2, IKT 6, and IKT 25, which had estimates of the progenitor mass based on X-ray observations, our SFH mass estimates are consistent with these values. Previous work on 1E 0102.2-7219 suggested that the SNR had a 25-35 M_{\odot} progenitor (Blair et al. 2000), whereas our SFH method has difficulty distinguishing the progenitor mass due to multiple peaks in the SFR in the last 50 Myr. However, our results showed that 49% of CC progenitors in the vicinity of 1E 0102.2–7219 are >21.5 M_{\odot} , and 31% of CC progenitors are $8-12.5 M_{\odot}$. Multiwavelength studies by Park et al. (2003) indicated that the progenitor of IKT 23 was an \sim 18 M_{\odot} star, based on a comparison of the SNR's abundances (O/Ne, O/Mg, and O/Si) to the model predictions of Nomoto et al. (1997). However, the nearby stellar population suggests that 100% of the CC progenitors arose from stars of 8–12.5 M_{\odot} . We note that if one compares the SNR's abundance ratios to updated SN II nucleosynthesis models from Sukhbold et al. (2016), then the ratios are consistent with an $\sim 15~M_{\odot}$ progenitor. Thus, in some cases, complementary optical and

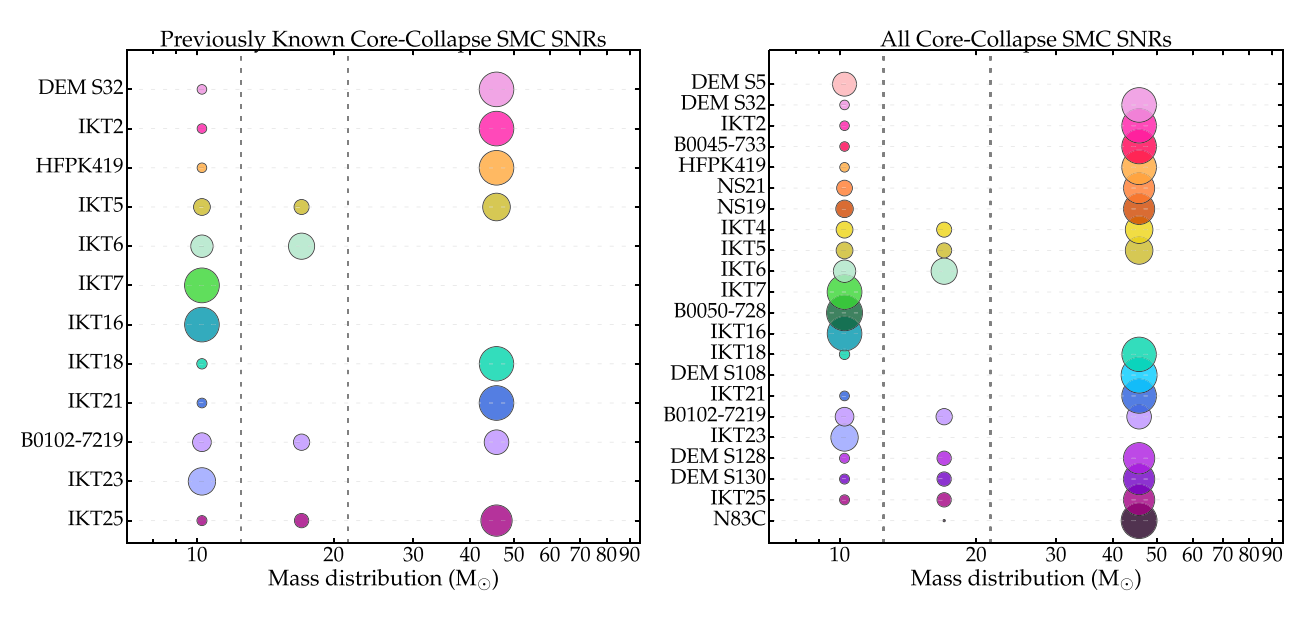


Figure 6. Left: mass distribution of the previously classified CC SMC SNRs listed in Section 5.1. Right: all SNRs classified as CC in our analysis, assuming a CC DTD arising from a binary stellar population and a Salpeter IMF. The size of the plot marker corresponds to how likely it is that the SNR was formed by a progenitor of mass 8–12.5, 12.5-21.5, and $>21.5~M_{\odot}$, assuming a binary-star population. These plots visually represent the numbers given in Table 2, with larger circles indicating greater likelihood, while no plot marker indicates a likelihood of zero. A similar trend is seen if one assumes a CC DTD and single-star population.

X-ray observations are crucial to differentiate the progenitor masses obtained from the SFH.

6.2. The IMF

Based on various studies of SNe and SNRs in nearby galaxies (e.g., Jennings et al. 2014; Williams et al. 2014a; Smartt 2015; Díaz-Rodríguez et al. 2018 and references therein), an absence of progenitors with mass $\gtrsim 18 M_{\odot}$ is apparent, suggesting a possible upper limit to the mass that produces observable CC SNe. Theoretically, this lack of progenitors above $\gtrsim 18\,M_{\odot}$ could be a natural result of the fact that a fraction of massive stars are expected to implode and form a black hole without a visible SN (e.g., Heger et al. 2003; Sukhbold et al. 2016). This suggestion was supported by the discovery of the disappearing $\sim 25 \, M_{\odot}$ red supergiant in NGC 6946 that likely underwent a failed SN (Gerke et al. 2015; Adams et al. 2017). However, recent studies by Maund (2017, 2018) of the resolved stellar populations around Type IIP and stripped-envelope SNe, as well as the discovery of a possible progenitor system for Type Ic SN 2017ein (Kilpatrick et al. 2018), suggest that even progenitors $\gtrsim 18 \, M_{\odot}$ can produce observable explosions. However, due to a number of factors discussed in Smartt (2015), the discovery rate of progenitor stars associated with SNe is small.

Nevertheless, combined with the properties of the SNR and its environment, the SFHs associated with these remnants provide a complementary and independent means to quantify the mass of CC progenitors. Based on our analysis, Figure 6 suggests that a large fraction of the SMC's CC progenitors result from high-mass progenitors, a result that contrasts the discoveries of pre-explosion SN progenitors (e.g., Smartt 2015) and studies of the SFH around SNRs in the high-metallicity galaxies M31/M33 (e.g., Jennings et al. 2014; Díaz-Rodríguez et al. 2018).

To probe this tension further, we investigate whether the SFHs at the sites of the SNRs yield a larger fraction of highmass stars than would be expected from the SFH of the SMC as a whole. To do this, we sum the SFHs at the locations of the SNRs and convolve the stacked SFH with the recent CC DTD of Zapartas et al. (2017) and a Salpeter IMF. This method yields the number of stars formed as a function of look-back time, and we convert look-back time to progenitor mass using the single-star models of Zapartas et al. (2017). This calculation then gives us the number of stars in each mass bin associated with the SNRs and the SMC as a whole. Figure 7 (left panel) plots the fraction of stars in each mass bin (i.e., the number of stars in a mass bin divided by the total number of stars with masses between ~ 8 and $70 M_{\odot}$) for previously identified CC SNRs (purple triangles) and all of the CC SNRs from this study (orange circles). The uncertainties in this fraction are derived from the uncertainty in the SFHs. Comparing the stacked SNR results to those of the SMC as a whole (cyan shaded region), we find that within the errors, these values are consistent. As such, our analysis is not biased toward identifying more massive progenitors than in the SMC as a whole.

In Figure 7 (right panel), we have plotted the cumulative progenitor mass distribution of the previously known CC SNRs listed in Table 2 and all SNRs classified as CC in our analysis as derived from their local SFHs. For reference, we include the corresponding cumulative distributions assuming a Salpeter IMF $(dN/dM \propto M^{-2.35})$ integrated to $120 M_{\odot}$ and the inferred mass distribution of the SNRs in M31 and M33 $(dN/dM \propto M^{-2.96})$; Jennings et al. 2014; Díaz-Rodríguez et al. 2018).

We note that the mass distribution of the SNRs in the SMC is similar to that of a Salpeter IMF but not as steep as that seen in M31 and M33, which has fewer high-mass progenitors (Jennings et al. 2014; Díaz-Rodríguez et al. 2018). Assuming that the mass distribution of all of the SMC SNRs can be well approximated using a power-law function of a form similar to that of the Salpeter IMF, we find that it can be well described using $dN/dM \propto M^{-1.84}$ (or $dN/dM \propto M^{-1.78}$ for the previously known CC SNRs). This result implies that the SMC

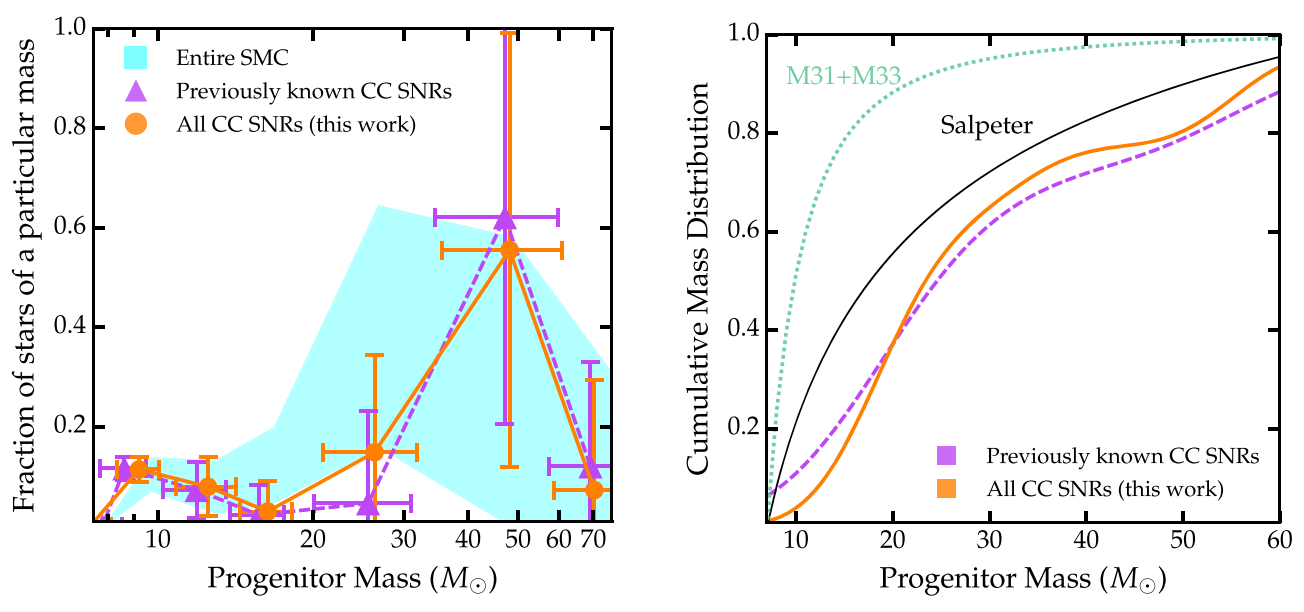


Figure 7. Left: fraction of SN progenitors of a particular mass associated with the previously known CC SNRs (purple triangles) and all SNRs classified as CC in our analysis (orange circles). To derive this, we convolved the stacked SFHs of each population with the recent CC DTD from Zapartas et al. (2017) and a Salpeter IMF. Here the error bars correspond to the 1σ uncertainty in this fraction as derived from the uncertainties in the SFHs. The cyan shaded region corresponds to the 1σ uncertainty in this fraction of SN progenitors of a particular mass, assuming the average SFH of the entire SMC. One can see that the number of SN progenitors associated with the SNRs in the SMC is consistent with the fraction derived from the SFH of the entire SMC, implying that we are not overly biased in our analysis toward measuring more massive stars. Right: cumulative progenitor mass distribution derived using the previously known CC SNRs listed in Table 2 (purple dashed line) and all SNRs classified as CC in our analysis (orange dashed line). In addition, we include the equivalent distributions for a Salpeter IMF integrated to $120 M_{\odot}$ (black solid line) and the inferred mass distribution for M31 and M33 (green dotted line; Jennings et al. 2014; Díaz-Rodríguez et al. 2018). One can see that the mass distribution for the SMC is similar to that of a Salpeter IMF but shallower than that seen in M31 and M33.

progenitor mass distribution is more top-heavy than M31 and M33, with higher-mass stars successfully producing a CC SN.

Assuming that a Salpeter IMF is representative of the stellar distributions, our results suggest that SNRs, at least in the SMC, are associated with higher-mass ($>21.5 M_{\odot}$) progenitors. A similar conclusion is reached when one considers the progenitor mass estimates from the X-ray and optical properties of individual SNRs. For example, studies of the SMC SNRs IKT 25 and 1E 0102.2-7219 indicated progenitors with masses $>25 M_{\odot}$ (Blair et al. 2000; Lopez et al. 2014a), and the same tension is found with both LMC and Milky Way SNRs (e.g., G292.0+1.8, Park et al. 2004; G54.1+0.3, Temim et al. 2010; Gelfand et al. 2015; W49B, Lopez et al. 2013; MSH 11-61A, Auchettl et al. 2015; N49B, Park & Bhalerao 2017; N132D, Blair et al. 2000; Plucinsky et al. 2018). In contrast to these results, studies by, e.g., Jennings et al. (2014) and Díaz-Rodríguez et al. (2018) found that the progenitor distribution of SNRs in M31 and M33, whose metallicity is higher than that of the SMC, is steeper than that of a Salpeter IMF based on the SFHs near the CC SNRs in those galaxies (see Figure 7, right panel).

The fact that SNRs in the SMC are associated with more massive progenitors, suggesting that higher-mass stars produce successful explosions, is also supported by recent theoretical work (e.g., Heger et al. 2003; Sukhbold & Woosley 2014; Pejcha & Thompson 2015; Sukhbold et al. 2016). These authors showed that the outcome of a CC SN of a particular mass depends nonmonotonically on the pre-SN core structure of the massive star. By investigating the explosive outcomes of a wide variety of masses, these authors found that there is no single initial mass below which all stars explode and produce a neutron star or above which all stars implode to a black hole. Rather, there are islands of explodability, in which even high-

mass progenitors may explode and produce an observable remnant. As a consequence, SNRs may be expected to be associated with a wide variety of progenitor masses.

6.3. The Effect of Metallicity on the IMF

It has been suggested that low-metallicity environments tend to favor a more top-heavy IMF (e.g., Schneider et al. 2002; Bromm & Larson 2004; Marks et al. 2012). In these environments, the metal-poor molecular clouds are very efficient in forming massive stars, since cooling via line emission or dust cooling, as well as fragmentation, is inefficient, resulting in higher-mass stars. (e.g., Padoan & Nordlund 2002; Bromm & Larson 2004; Bate & Bonnell 2005; Larson 2005; Marks et al. 2012). However, even though understanding the effect of metallicity on the mass distribution of progenitors is fundamentally important for the theory of SF, its current dependence is not well constrained in the literature (see review by Bastian et al. 2010). However, there is increasing observational evidence that favors an IMF shallower than Salpeter in metal-poor environments such as those seen in ultrafaint dwarf (e.g., Dabringhausen et al. 2012; Geha et al. 2013) and early-type galaxies (Martín-Navarro et al. 2015).

6.4. The Effects of Mass Loss, Rapid Rotation, and Binary Interaction on the IMF

Apart from metallicity, both mass loss via stellar winds and binary interaction play an important role in altering the shape of the measured IMF (e.g., Schneider et al. 2015). For single-star populations, two effects change the observed IMF of this population: stellar wind mass loss (which is dependent on the metallicity of the environment and the mass of the star) and when stars of a particular mass leave the main sequence (which

translates into the slope of the IMF). Schneider et al. (2015) found that as stellar mass loss increases (which occurs with increasing mass and metallicity), the measured IMF of this population becomes more top-heavy.

For binary-star populations, two additional processes alter the observed mass function of these objects: stellar mergers (e.g., Bonnell et al. 1998) and mass exchange between binary components via Roche lobe overflow (e.g., Kippenhahn & Weigert 1967). Both of these processes tend to shift the stars toward higher masses (Schneider et al. 2015) while also making the mass gainer (or merger product) appear younger, since the fraction of burnt fuel decreases as fresh hydrogen is introduced in the core (e.g., Dray & Tout 2007 and reference therein). These rejuvenated binary products can make up nearly one-third of the stars $>40 M_{\odot}$, but this fraction decreases as both the number of binary systems and the mass of the binary products decrease (Schneider et al. 2015). As the amount of mixing will increase with greater mass and rotation rate and decreased metallicity (e.g., Brott et al. 2011; de Mink et al. 2013; Schneider et al. 2014), this effect will be more pronounced in low-metallicity environments like the SMC. Unresolved binaries also tend to make the observed mass function more top-heavy (e.g., Weidner et al. 2009; Schneider et al. 2015), with this shift being strongest at larger stellar masses, assuming a constant IMF slope. However, unresolved binaries tend to flatten the mass function less than resolved binaries.

Assuming constant SF, de Mink et al. (2014) showed that $\sim 30\%$ of massive main-sequence stars are the products of binary interaction. Thus, they contribute a nonnegligible fraction to the stellar populations measured to derive SFHs like that used in this study. However, most studies that calculate the SFH from a stellar population do not include interacting binaries, or they use an ad hoc binary fraction in which secondary masses are drawn randomly from an IMF. However, work such as that of Eldridge et al. (2017) has shown that the SFHs derived using single stars only tend to peak somewhat earlier and not as strongly as the SFHs derived assuming a binary DTD (see Figure 27 of Eldridge et al. 2017). As such, ignoring interacting binaries can lead to incorrect SFHs being deduced.

In total, 13 of the SMC SNRs have stellar populations that show evidence of bursts of SF of various intensities \sim 50–200 Myr ago (Figure 5) and properties suggestive of CC origin. The additional burst of SF ~50-200 Myr ago may hint toward evidence of delay CC SN timescales due to binary interaction. To quantify this, we use the CC DTD assuming the binary stellar population of Zapartas et al. (2017) to estimate the possible delay CC contribution. Here we assume that the \sim 50–200 Myr peak results solely from massive progenitors undergoing CC; this allows us to estimate an upper limit of this contribution, which we list in Table 2. We find that for most of the remnants, <8% of the stellar population could come from a delayed CC as a result of binarity. However, for DEM S5 and IKT 23, we find that a large fraction of the stellar population could have arisen from a delayed CC. As the properties of IKT 23 and DEM S5 suggest that these source result from a CC event rather than a Type Ia SN, it is possible that these remnants arose from a delayed CC.

A natural consequence of binarity is that a large fraction of these massive stars will be rapidly rotating (de Mink et al. 2013). Detailed studies of stars in the SMC and LMC indicate

that some stars are rotating much faster than those found in the Milky Way (e.g., Martayan et al. 2007; Golden-Marx et al. 2014; Bastian et al. 2017; Dupree et al. 2017). De Mink et al. (2013) suggested that $\sim\!20\%$ of massive main-sequence stars rotate rapidly due to binary interaction, while most, if not all, rapidly rotating stars are likely the result of mass transfer in these binaries. Under this assumption, they found that they could naturally explain the observed rotational distribution of stars in these samples. Rapid rotation increases chemical mixing within the interior of the star, which increases the fuel available to that star and naturally extends its lifetime (Sreenivasan & Wilson 1982; Pols et al. 1998; Maeder & Meynet 2000) to $\sim\!50$ –200 Myr.

We should also note that the SMC is known to be highly efficient in forming high-mass X-ray binaries (HMXBs) that consist of a neutron star orbiting a rapidly rotating B-type main-sequence star (e.g., Shtykovskiy & Gilfanov 2005; Haberl & Sturm 2016). This characteristic is consistent with evidence that binary interaction (and to some extent, low metallicity) favors the formation of rapidly rotating stars (e.g., Dray 2006; Antoniou et al. 2010; Douna et al. 2015; Haberl & Sturm 2016).

6.5. The Ratio of CC to SN Ia Progenitors

To quantify the likelihood that each SNR in our sample arises from a CC or SN Ia progenitor, we convolve the local SFH of each SNR with the Type Ia DTD of Maoz & Graur (2017) plus a CC DTD assuming either a single or binary stellar population from Zapartas et al. (2017). To be consistent with the previous study of the resolved local SFH around SNRs in the LMC (Maoz & Badenes 2010), we divide the SFH of each SNR into three time bins: <35 Myr, 35-330 Myr, and 330 Myr-14 Gyr. These bins represent the timescales of CC SNe, delayed CC SNe and prompt SNe Ia if one assumes binary-star models, and delayed SNe Ia, respectively. To determine the ratio of expected CC to SN Ia progenitors $(N_{\rm CC}/N_{\rm Ia})$, we integrate the SFH in each bin to derive the mass formed at each timescale and multiply this value by the Type Ia + CC SNe DTD. Here we have assumed that the distribution of stellar ages is representative of the stellar distribution when the original star underwent an SN. In Table 2, we list the local $N_{\rm CC}/N_{\rm Ia}$ for each SNR assuming both a single- and binary-star population DTD for the CC SN.

Before convolving the Type Ia + CC SN DTD with the SFH associated with each SNR, we convolved our DTD with the total Z = 0.008 stellar mass formed in the SMC (Figure 2, left panel) to derive the ratio of CC to SN Ia progenitors for the SMC. We find $(N_{\rm CC}/N_{\rm Ia})_{\rm SMC} \sim 6$, assuming both a single and binary stellar population. This ratio is similar to that derived from local SN surveys and in galaxy clusters. Using a volumelimited SN sample, Li et al. (2011) and Holoien et al. (2017) showed that $N_{\rm CC}/N_{\rm Ia}\sim3$; de Plaa et al. (2007) and Sato et al. (2007) estimated $N_{\rm CC}/N_{\rm Ia}\sim 2$ –4 based on elemental abundances in the intracluster medium from X-ray observations of galaxy clusters. Additionally, Tsujimoto et al. (1995) derived $N_{\rm CC}/N_{\rm Ia} \sim 3-6$ for the solar neighborhood and the Magellanic Clouds using the observed elemental abundances and comparing them to galactic models of chemical evolution. More recently, Maggi et al. (2016) estimated $N_{\rm CC}/N_{\rm Ia} \sim 1.2$ –1.8 for the LMC, assuming that the number of observed LMC SNRs is representative of the CC/Ia SN rates.

Maggi et al. (2016) suggested that the discrepancy between the LMC $N_{\rm CC}/N_{\rm Ia}$ ratio and those derived from local SN surveys and the intracluster medium is a result of the unique SFH of the Magellanic Clouds (which have had several distinct epochs of active SF). However, in their original study, Maggi et al. (2016) did not utilize a DTD in their analysis when attempting to interpret the local SFH of each LMC remnant in terms of an SN progenitor. As such, it is possible that their $N_{\rm CC}/N_{\rm Ia}$ ratio is underestimated, and in reality, the $N_{\rm CC}/N_{\rm Ia}$ ratio for the LMC is consistent with the observational studies listed above.

For each SNR in the SMC, their SFH suggests $N_{\rm CC}/N_{\rm Ia} > 1$, implying that these remnants are associated with stellar populations that favor a CC progenitor over that of a Type Ia. Among the sources that have $N_{\rm CC}/N_{\rm Ia} < (N_{\rm CC}/N_{\rm Ia})_{\rm SMC}$, where $(N_{\rm CC}/N_{\rm Ia})_{\rm SMC} \sim 6$, IKT 6 has an associated neutron star, IKT 23 and 1E 0102.2–7219 are oxygen-rich CC SNRs, and DEM S5 and NS 21 are located near H II regions. Consequently, the properties of these SNRs are more consistent with those of CC SNe than SNe Ia. Implying a preference for CC over that of Type Ia progenitors, HFPK 334 has one of the lowest ratios $(N_{\rm CC}/N_{\rm Ia} \sim 3)$. Based on its low-density environment (see Section 5.3) and its SFH, which is distinct from all other SNRs in our sample, we believe HFPK 334 likely arose from an SN Ia. Another possibility is that this SNR arose from a delayed CC SN.

6.6. Selection Effects

One remarkable result from our analysis is that nearly all (22/23) remnants in the SMC have SFHs and properties consistent with CC events. The four SNRs (IKT 4 [SNR J0048.4–7319], IKT 5 [SNR 0047–73.5], IKT 25 [SNR 0104–72.3], and DEM S128 [SNR 0103–72.4]) suggested to arise from SNe Ia in the literature all have properties, local SFHs, and $N_{\rm CC}/N_{\rm Ia}$ indicative of CC explosions. However, it is noteworthy that $(N_{\rm CC}/N_{\rm Ia})_{\rm SMC}$ is lower than that implied by our classifications of the SNR sample $(N_{\rm CC}/N_{\rm Ia}=22/1)$. For the SMC SNRs to have $(N_{\rm CC}/N_{\rm Ia})_{\rm SMC}\sim 6$, it should have $\sim 3-4$ Type Ia SNRs (out of 23 known SNRs), which is lower than that suggested from our analysis.

The discrepancy between the high $N_{\rm CC}/N_{\rm Ia}$ of the SMC implied by Table 2 and the measured $(N_{\rm CC}/N_{\rm Ia})_{\rm SMC}\sim 6$ arises from the scarcity of identified Type Ia SNRs in the SMC. Kobayashi et al. (1998) and Langer et al. (2000) suggested that the rates of SNe Ia are metallicity-dependent, with low-metallicity environments inhibiting SNe Ia because the wind of the accreting WD is too weak to reach the Chandrasekhar mass limit. However, SNe Ia are observed in low-metallicity galaxies (e.g., Prieto et al. 2008), and several studies have argued that the Type Ia rate should increase as metallicity decreases because low-metallicity stars produce higher-mass WDs (Umeda et al. 1999; Meng et al. 2008; Kistler et al. 2013).

Recent work by Sarbadhicary et al. (2017) suggested that Type Ia SNRs may be more difficult to detect than CC SNRs in the SMC. These authors showed through semi-analytical modeling that a large fraction (~30%–40%) of Local Group SNRs are missed in current radio surveys. They found that most SNRs above detection limits will be CC SNRs, whereas Type Ia SNRs evolve in lower ambient densities and have lower surface brightnesses and thus shorter visibility times, which may preclude their detection.

This result naturally arises from the fact that the luminosity of a source is proportional to the square of the density n of the surrounding environment (e.g., Patnaude et al. 2015). As the massive progenitors of CC SNe tend not to travel far from their original birth sites due to their short lifetimes (Eldridge et al. 2011; Renzo et al. 2018), these sources are usually found in dense environments. As a result, these SNRs tend to be more X-ray bright than those found in low-density environments (e.g., Patnaude et al. 2015).

In addition, the prevalence of CC SNRs in the SMC may be a natural result of the mass-loss properties of the progenitors implied by the SFHs. As the mass-loss rate (\dot{M}) increases, the X-ray luminosity of stellar ejecta and swept-up material will scale as \dot{M}^2 (e.g., Patnaude et al. 2015). As higher-mass progenitors tend to lose more mass prior to explosion, the X-ray luminosity of those SNRs will be significantly brighter than those resulting from lower-mass progenitors. Thus, these SNRs will be detected more readily, introducing a selection effect that SNRs detected in X-rays arise from higher-mass CC SN progenitors.

However, we note that n naturally influences the observable lifetimes of SNRs. The SNR evolution is described as three distinct stages: first is the free expansion phase, where the shock front travels unimpeded by the surrounding environment (Chevalier 1982; Truelove & McKee 1999). Subsequently, the Sedov-Taylor phase (Taylor 1950; Sedov 1959) occurs when the mass of swept-up material is comparable to the mass of the ejecta, causing the forward shock to decelerate and producing a reverse shock that heats the inner ejecta to Xray-emitting temperatures (McKee 1974). This phase ends when radiative cooling becomes dynamically important and the remnant enters the snowplow phase (McKee & Ostriker 1977) before disappearing. The transition between the Sedov-Taylor phase and the radiative snowplow stage occurs at $t = 2.9 \times 10^4 E_{51}^{4/17} n^{-9/17}$ yr (where $E_{51} \equiv E/10^{51}$ erg is the explosion energy; Blondin et al. 1998) and can be used as an approximate lifetime of the SNR. Assuming $E_{51} = 1$, the lifetime of an SNR in a dense environment will be shorter than one in a low-density environment. As a result, CC SNRs arising from more massive progenitors are likely to be brighter than those from lower-mass progenitors but tend to have much shorter lifetimes.

Since the original *XMM-Newton* X-ray (Haberl et al. 2012a) and ATCA radio (Payne et al. 2004; Filipović et al. 2005) surveys of the SMC are quite shallow, ¹¹ it is possible that we are currently biased toward detecting the remnants from the highest-mass progenitors, while some fraction of SNRs are below detection limits. In fact, it was shown by, e.g., Chomiuk & Wilcots (2009) that current radio SNR surveys are sensitivity-limited. Thus, our results may suggest that the SNR sample in the SMC is incomplete, and a deeper, systematic study of the SMC at multiple wavelengths would be beneficial to identify and characterize the full SNR population.

7. Conclusion

In this paper, we present a systematic study of the stellar populations in the vicinities of 23 known SNRs in the SMC.

 $[\]overline{\ ^{11}}$ The *XMM-Newton* survey covered the galaxy with an effective exposure of $\sim\!\!25$ ks field $^{\!-1}$, corresponding to a flux limit of $\sim\!\!10^{-14}$ erg s cm $^{\!-1}$ (Haberl et al. 2012a). The ATCA survey of the SMC observed SNRs down to a flux of $\sim\!\!2\times10^{16}$ W Hz $^{\!-1}$ at 1.42 GHz (Payne et al. 2004; Filipović et al. 2005).

Combined with the properties of the remnants themselves and their surrounding environment, we investigate the SFH at the sites of the SNRs, and we infer the natures of the SN progenitors based on the time since peaks in the SFR. The explosive origins of many SMC SNRs have not been characterized previously, and the SFHs reveal the likelihood of whether individual sources arise from a CC or SN Ia. We find that nearly all known SNRs (22/23) have local SFHs and properties consistent with CC SNe, including four remnants that had previously been classified as Type Ia SNRs in the literature based on their X-ray properties. The scarcity of Type Ia SNRs may be because these sources are visible for much shorter times than CC SNRs and are intrinsically less luminous (Sarbadhicary et al. 2017), or that CC remnants tend to be easier to detect due to the nature of their progenitor.

By convolving the local SFHs of each remnant with recent single and binary stellar population CC DTDs, we estimate the mass distribution of CC progenitors in the SMC. We find that this distribution is consistent with a standard Salpeter IMF but shallower than that measured in M31 and M33 using similar methods, implying that SNRs in the SMC are associated with more massive stars. This is consistent with individual X-ray and optical studies of particular SMC SNRs (e.g., IKT 25 and 1E 0102.2-7219), which had suggested large progenitor masses ($\sim 25~M_{\odot}$) for these remnants previously. The topheavy mass distribution suggested by these works contrasts the progenitor masses of \lesssim 18 M_{\odot} estimated from stellar population studies around SNRs and pre-explosion images of SNe in nearby galaxies. However, recent theoretical work by, e.g., Sukhbold & Woosley (2014), Pejcha & Thompson (2015), and Sukhbold et al. (2016) has shown that there is no single mass below or above which a progenitor will explode or implode, with even progenitor masses $\gtrsim 18 \, M_{\odot}$ able to produce observable explosions.

Furthermore, we show that a large fraction of the SMC SNRs exhibited a burst of SF between 50 and 200 Myr ago. For example, the oxygen-rich SNR IKT 23 likely had a massive progenitor, and its peak SF occurred ~50–200 Myr ago. As such, it is possible that IKT 23 and other SMC SNRs had progenitor stars with extended lifetimes due to either their environments or binarity. As most of these sources have properties and SFHs consistent with CC origins, we suggest that the long massive star lifetimes may be a product of binary interaction and rapid rotation (e.g., Brott et al. 2011; de Mink et al. 2013; Schneider et al. 2015; Zapartas et al. 2017) or the low-metallicity environment of the SMC (e.g., Sreenivasan & Wilson 1982; Pols et al. 1998; Maeder & Meynet 2000).

We thank the referee for the very detailed and insightful review that helped improve both the quality and clarity of the work presented. We thank Nicole Man, Marc Pinsonneault, and Jeremiah Murphy for their helpful discussions. L.A.L. gratefully acknowledges that this work was supported through NSF Astronomy & Astrophysics grant AST-1517021 and acknowledges support from the Sophie and Tycho Brahe Visiting Professorship at the Niels Bohr Institute. C.B. is supported by grants NSF/AST-1412980 and NASA ADAP NNX15AM03G-S01. E.R.R. is supported by the David and Lucile Packard Foundation and the Danish National Research Foundation through a Niels Bohr Professorship. J.F.B. is supported by NSF grant PHY-1714479.

Appendix A Properties of the SNRs in the SMC

DEM S5 (B0039-7353, HFPK 530, SNR J0040.9-7337, SNR J004100-733648). One of the largest SNRs (diameter \sim 60 pc) in the SMC, DEM S5 was first classified as an SNR based on the detection of X-ray emission from the position of an emission nebula from ROSAT (Kahabka et al. 1999; Haberl et al. 2000). Its SNR origin was later verified by Filipović et al. (2005) and Payne et al. (2007) using ATCA. This source has a complex optical shell comprised of two intersecting shells, and bright [O III] emission suggests that the SNR shock front is traveling with $v > 100 \,\mathrm{km \, s^{-1}}$. Shallow XMM-Newton observations of this source detected faint X-ray emission coincident with bright H α and [S II] emission, implying that the SNR is interacting with dense material (Filipović et al. 2008). Due to the shallowness of the XMM-Newton observation and low surface brightness of the source, no abundance measurements have been constrained, although its size, low temperature, and ionization timescale indicate an old age (Filipović et al. 2008). As of this writing, no attempt has been made to characterize the progenitor type of this remnant.

The SFH of DEM S5 indicates that the SNR is located in an active star-forming region of the SMC. The SFH is dominated by metal-rich SF \sim 50 Myr ago, with a smaller peak \sim 30 Myr ago. A low-metallicity SF event occurred \sim 100 Myr ago. Assuming that the SNR arose from a CC SN, 100% of the progenitors have masses of 8–12 M_{\odot} . We note that significant SF happened \sim 50–200 Myr ago, which may imply that a large fraction (56%) of the progenitors associated with this remnant underwent delayed CC. If DEM S5 arose from a Type Ia SN, then a prompt progenitor is favored for this source, given the low SFR at look-back times >100 Myr. Follow-up observations of DEM S5 are necessary to confirm the nature of the progenitor.

DEM S32 (*SNR J0046.6–7309*). After this source was detected in a number of X-ray surveys of the SMC, van der Heyden et al. (2004) obtained a pointed XMM-Newton observation of DEM S32. They found significant thermal X-ray emission with evidence of emission lines from O, Ne, Si, Fe, and possibly Mg. Assuming a Sedov model of SNR evolution (Sedov 1959), they estimated that the SNR is \sim 6 kyr old and has swept up ${\sim}43\,M_{\odot}$ of material. Due to its location close to large nebula N19 (Henize 1956; Dickel et al. 2001), van der Heyden et al. (2004) suggested that the SNR was a CC explosion. This source is located in the same SF subcell as HFPK 419 and IKT 2. As a consequence, this source has the same SFH reported here as those SNRs. According to our estimates from the SFH, this SNR most likely arose from a $>21.5 M_{\odot}$ progenitor that underwent a Type IIP explosion, similar to HFPK 419.

IKT 2 (SNR J0047.2–7308, HFPK 413, B0045–73.4). Detected across radio wavelengths (e.g., Dickel et al. 2001; Payne et al. 2004; Lee et al. 2009), this source was first studied in X-rays by Yokogawa et al. (2002) using ASCA. They found that the X-ray morphology is center-filled and highly irregular, and the X-ray emission has enhanced abundances of Ne and Mg consistent with a progenitor of $\sim 20~M_{\odot}$. Using ROSAT and XMM-Newton, Dickel et al. (2001) and van der Heyden et al. (2004) found that the X-ray emission from IKT 2 is best described by a thermal plasma model with enhanced Ne, Mg, Si, and possibly Fe, suggesting an ejecta origin for the emission. Van der Heyden et al. (2004) derived a Sedov age for

the SNR of \sim 5.6 kyr, and they classified the SNR as being from a CC explosion based on enhancement of intermediatemass elements and location near the nebula N19. By comparing their abundance measurements to SN explosion models, Yokogawa et al. (2002) concluded that the SNR most likely arose from an $\sim 20\,M_{\odot}$ progenitor. Using *Chandra*, Williams et al. (2006) detected hard X-ray emission within the remnant, possibly from a PWN. It was originally suggested that both IKT 2 and HFPK 419 were one remnant due to their proximity, but van der Heyden et al. (2004) showed based on their X-ray properties that these sources are distinct. Found in the same subcell as HFPK 419 and DEM S32, this SNR exhibits the same SFH as the two other remnants. This SNR is located within the nebula N19, which is associated with moderate starburst activity (Dickel et al. 2001). From the SFH, 92% of the CC SN progenitors in this region are from stars $>21.5 M_{\odot}$. This value is slightly greater than the progenitor mass of 20 M_{\odot} suggested by Yokogawa et al. (2002), but it is consistent within their errors. If the pulsar wind nebula identified by Williams et al. (2006) is confirmed, then this result is consistent with the models of Sukhbold et al. (2016), which suggested that neutron stars are produced in SNe of stars $<30 M_{\odot}$.

B0045-733 (HFPK 401, SNR J0047.5-7306). This compact (~13 pc in diameter) SNR was first detected in X-rays by Haberl et al. (2012a) using XMM-Newton. Due to its low surface brightness, there is little known about its properties; however, Filipović et al. (2005) and Payne et al. (2007) detected [O II] and Hβ emission from the source, confirming its SNR nature. The SNR is located near star-forming nebula N19 and found in the same subcell as HFPK 419, DEM S32, and IKT 2. As such, B0045-733 has the same SFH as reported for these SNRs, with significant metal-rich SF around ~5 and ~30 Myr ago, consistent with a CC origin. Assuming a CC event, 92% of progenitors in this region arose from stars >21.5 M $_{\odot}$.

HFPK 419 (SNR J0047.7-7310). Overlapping SNR IKT 2, this source is located within the emission nebula N19, which is thought to be associated with modest starburst activity (Dickel et al. 2001). The SNR is located in a part of N19 that had a period of intense, metal-rich (Z = 0.008) SF ~ 5 Myr ago, as well as another burst ~ 30 Myr ago (see Figures 4 and 5). The region has had minimal SF activity aside from these events. Van der Heyden et al. (2004) suggested that the SNR originated from a CC SN based on detection of enhanced Ne and Mg relative to Si and Fe, but they did not constrain a progenitor mass or whether the X-ray emission arose from ejecta or ISM material. The asymmetric X-ray morphology of the SNR (see Figure 2 of van der Heyden et al. 2004) is also consistent with a CC event (e.g., Lopez et al. 2009a, 2009b, 2011). Van der Heyden et al. (2004) estimated a Sedov age of ~ 8.5 kyr for this remnant. Based on the SFH there (assuming a single-star population), it is expected that the majority (92%) of the CC SN progenitors in the subcell have a mass $>21.5 M_{\odot}$, with the other 8% having masses of $8-12.5 M_{\odot}$. As per the classifications defined in Section 4.2, this result suggests that the SNR arose from either a Type IIP or a Type Ib/Ic SN. However, as only a shallow XMM-Newton observation is available of HFPK 419 (van der Heyden et al. 2004), further study is warranted to confirm the nature of this source.

NS 21 (DEM S35, SNR J0047.8-7317). This radio-detected SNR is associated with the H II region DEM S35

(Filipović et al. 2005; Pellegrini et al. 2012). Haberl et al. (2012a) detected no X-rays arising from the position of NS 21 in their XMM-Newton survey of the SMC. Studying the lifetime and destruction efficiencies of silicate and carbon dust in the Magellanic Clouds, Temim et al. (2015) found that the dust-togas ratio surrounding this source is enhanced, implying a dense environment. The SFH of NS 21 is similar to that of IKT 4 and IKT 5, which are located nearby. The SFH has a peak of metalrich SF ~9 Myr ago and extended, metal-rich SF from \sim 30–1000 Myr ago. Assuming that the SNR arises from a CC SN, 22% of CC progenitors would be 8–12.5 M_{\odot} stars, and 78% would be stars $> 21.5 M_{\odot}$. Assuming a Salpeter IMF, 34% of stars would have $>40 M_{\odot}$. A strong peak of SF is exhibited by NS 21 in the 50-200 Myr bin, which could be a signature of delayed CC. However, if NS 21 is a Type Ia SN, then we find that 99% of progenitors are prompt and 1% are delayed. Deep X-ray observations of NS 21 to measure the plasma abundances would be beneficial to constrain the nature of the SNR.

NS 19 (*DEM S31*, *SNR J0048.1−7309*). No X-ray emission has been detected that is coincident with the optical emission from NS 19. However, Haberl et al. (2012a) detected a larger, elliptically shaped source of X-ray emission that may be related to the SNR. The radio emission of the source arises from the southwest portion of the remnant (Filipović et al. 2005); however, contamination from a nearby H II region (Dickel et al. 2001) makes it difficult to disentangle the SNR properties. It is located near the SNRs HFPK 419, DEM S32, and IKT 2 and the N19 star-forming region. The SFH of NS 19 is similar to that of the nearby remnants, with SF peaks at ~5 and ~30 Myr ago. Based on our estimates, 26% of the CC progenitors are stars with masses between 8 and $12\,M_{\odot}$, while 74% arise from stars with masses >21.5 M_{\odot} . Using a Salpeter IMF, 34% of >21.5 M_{\odot} stars will be >40 M_{\odot} .

IKT 4 (HFPK 454, SNR J0048.4—7319). Using XMM-Newton, van der Heyden et al. (2004) found that the X-ray emission from IKT 4 peaks in the 0.7–1.0 keV band, implying that its emission is dominated by Fe-L emission. Van der Heyden et al. (2004) showed that the X-rays arise from a smaller radius than the optical emission of this source (Mathewson et al. 1984), suggesting it is an old SNR. These authors were unable to estimate the elemental abundances because the SNR is faint in X-rays, but the Fe-L emission may indicate a Type Ia explosive origin. As IKT 4 is found in the same subcell as IKT 5, it has the same SFH, with extended but intense SF <50 Myr ago. More details of its SFH can be found in Section 5.2.

IKT 5 (DEM S49, HFPK 437, B0047-735, SNR 0047-73.5, SNR J0049.1-7314). This radio-dim SNR (Mathewson et al. 1984) was first discovered in soft X-rays using the Einstein Observatory (Inoue et al. 1983). Deep, follow-up observations using XMM-Newton and Chandra by van der Heyden et al. (2004) and Roper et al. (2015), respectively, found extended X-ray emission that is best described by a thermal plasma model with possibly enhanced Ne, Mg, and Fe. They detected a point source coincident with IKT 5 but claimed it was most likely a star. Using ATCA, Roper et al. (2015) also found a radio half-shell coincident with the X-ray emission, which is connected via an optical shell (Payne et al. 2007). Both van der Heyden et al. (2004) and Roper et al. (2015) suggested a Type Ia origin based on the enhanced abundances. However, Roper et al. (2015) also suggested that this source may be from a CC given its environment and enhanced Ne and Mg abundances. Shtykovskiy & Gilfanov (2005) identified a hard X-ray point source at the remnant's center that is an HMXB candidate located near the SNR's geometric center (Shtykovskiy & Gilfanov 2005; K. Auchettl et al. 2019, in preparation). The vicinity of IKT 5 shows consistent, strong metal-rich SF for the last $\sim\!50\,\mathrm{Myr}$ with a peak SFR $\sim\!30\,\mathrm{Myr}$ ago. A burst of metalpoor SF occurred $\sim\!100\,\mathrm{Myr}$ ago. We find that 24% of CC progenitors are stars with masses of 8–12.5 M_{\odot} , 17% have a mass of 12.5–21.5 M_{\odot} , while 59% have masses $>\!21\,M_{\odot}$. Assuming a binary stellar population DTD, the enhanced SF seen between 50 and 100 Myr (Figure 5) suggests that 2% of the progenitors underwent delayed CC due to binarity.

IKT 6 (1E 0049.4—7339, HFPK 461, B0049—73.6, SNR J0051.1 -7321). IKT 6 was first discovered in X-ray surveys (Inoue et al. 1983; Wang & Wu 1992; Haberl et al. 2000) and followed up with XMM-Newton (van der Heyden et al. 2004), Chandra (Hendrick et al. 2005; Schenck et al. 2014), and Suzaku (Takeuchi et al. 2016). It exhibits a center-filled X-ray morphology with a distinct ringlike feature in projection that is surrounded by a larger, fainter, metal-poor shell. The SNR has enhanced O, Ne, Mg, and Si abundances in its center, indicating that the X-ray emission arises from ejecta. Van der Heyden et al. (2004), Hendrick et al. (2005), and Schenck et al. (2014) determined that the SNR is evolved, with a Sedov age of \sim 14-17 kyr. By comparing the properties of IKT 6 to other Type II SNRs in the SMC (e.g., IKT 22), van der Heyden et al. (2004) suggested that the SNR was from a CC explosion. More recently, Hendrick et al. (2005) and Schenck et al. (2014) suggested that this SNR resulted from an asymmetric CC SN of a 13-15 M_{\odot} progenitor with solar or subsolar (Z = 0.004) metallicity (Hendrick et al. 2005; Schenck et al. 2014) in a locally metal-poor environment. At the site of this SNR, significant SF has occurred at metallicities of Z = 0.004 and 0.008, with the latter dominating at look-back times $\gtrsim 10$ Myr. From 100 to 1000 Myr ago, the SF included a lower-metallicity (Z = 0.001 and 0.004) component, as well as the metal-rich component that contributed at look-back times \lesssim 500 Myr. Based on the Z = 0.008 SFH associated with IKT 6, 46% of the CC SN progenitors should be stars that have a mass of $8-12.5 M_{\odot}$, and 54% of the massive stars have a mass of $12.5-21.5 M_{\odot}$, assuming a single-star population. This result is consistent with the \sim 13–15 M_{\odot} progenitor suggested by Hendrick et al. (2005) and Schenck et al. (2014). We note that the SFH of IKT 6 has a strong peak in the 50–200 Myr bin. Assuming a binary-star population, this peak could indicate that 8% of progenitors underwent a delayed CC.

IKT 7 (HFPK 424, SNR J0051.9–7310). Inoue et al. (1983) classified IKT 7 as an SNR by using X-ray hardness ratios from the Einstein Observatory. Follow-up XMM-Newton observations by Haberl et al. (2012a) found that IKT 7 is associated with the 172 s Be/X-ray pulsar AX J0051.6-7311, originally identified with ASCA (Yokogawa et al. 2000). Filipović et al. (2008) and Haberl et al. (2012a) did not detect extended emission from the SNR, but the exposures were relatively short $(\sim 10-30 \text{ ks})$ in both studies. As a result, the nature of this SNR is uncertain; however, the SNR may be associated with a Be/ X-ray pulsar binary system, AX J0051.6-7311 (Yokogawa et al. 2000; Haberl et al. 2012a), indicating that the remnant has a CC origin. The region shows strong, metal-rich SF \sim 30 Myr ago, with weaker but still significant SF 100-500 Myr ago. Within the uncertainties, low-metallicity (Z = 0.004) SF may have occurred ~ 1 Gyr ago. Based on the SFH, we expect 100% of the CC SN progenitors to be stars with masses of 8-12.5 M_{\odot} . As Be/X-ray binaries contain B-star companions of mass $2{\text -}16\,M_{\odot}$, it is possible that the companion formed in the same population of stars as the progenitor of IKT 7. We note that significant SF occurred 50–200 Myr ago, with 7% of the stellar population undergoing delayed CC assuming a binary stellar population. If the Be/X-ray pulsar system is confirmed to be associated with this remnant, this could suggest that IKT 7 arose from a delayed CC. However, further follow-up of this source is warranted.

B0050–728 (DEM S68SE, HFPK 285, SNR J0052.6–7238, SNR J005240–723820, SMC 258, NS 76). Detected at both radio (Filipović et al. 2005) and optical (Payne et al. 2007) wavelengths, this very large SNR (diameter \sim 7′) shows significant thermal X-ray emission (Haberl et al. 2012a) and evidence of [O II], [S II], Hα, and Hβ (Payne et al. 2007). Haberl et al. (2012a) suggested that B0050–728 is either a large SNR or one of a pair of SNRs with similar temperatures. This source is located near the H II region N51 (Lopez et al. 2014b). The region's SFH exhibits an intense peak of metal-rich SF around \sim 40 Myr ago and little subsequent SF. The SFH resembles that of the CC SNRs, so it is possible that this source arose from a CC event. We estimate that all CC SN progenitors in the region have a mass of 8–12.5 M_{\odot} .

IKT 16 (HFPK 185/194, SNR J0058.3-7218). This source was first classified as an SNR using Einstein observations (Inoue et al. 1983) before its shell-type nature was confirmed by radio and H α observations by Mathewson et al. (1984). Using XMM-Newton, van der Heyden et al. (2004) found hard X-ray emission at the center of IKT 16. Owen et al. (2011) found strong evidence of a PWN in both X-ray and radio observations, and they estimated that the neutron star (NS) has a kick velocity of $580 \pm 100 \, \mathrm{km \, s^{-1}}$. Follow-up *Chandra* observations analyzed by Maitra et al. (2015) confirmed the presence of a PWN and constrained both the spectral and spindown properties of the source. Owen et al. (2011) found that the SNR is highly extended, with a radius of $37d_{60\text{kpc}}$ pc, making it one of the largest SNRs in the SMC. Owen et al. (2011) calculated the Sedov age of the SNR to be \sim 15 kyr. The detection of a PWN associated with the SNR implies that this remnant arises from a CC SN. The thermal X-ray emission from IKT 16 is faint, precluding an estimate of the progenitor mass based on its X-ray properties. Consequently, the SFH in its vicinity yields the first constraints on its progenitor star mass. The region had strong, metal-rich SF 20–100 Myr ago, followed by weak SF across all metallicities. Based on its SFH, the SNR likely arose from a progenitor of mass 8–12.5 M_{\odot} . Also, IKT 16 exhibits substantial SF around 50-200 Myr, which could imply that some of the stellar population associated with this remnant underwent delayed CC.

IKT 18 (1E 0057.6-7228, HFPK 148, NS 66, SNR J0059.4-7210). First detected using Einstein (Seward & Mitchell 1981; Inoue et al. 1983), this SNR is located close to the bright, young (~3 Myr old) star cluster NGC 346 (Filipovic et al. 1998) that powers the H II region N66 (Massey et al. 1989; Lopez et al. 2014b) and was confirmed as an SNR by Filipović et al. (2005) using ACTA. Coincident with IKT 18 is the multistar system HD 5980 (e.g., Sterken & Breysacher 1997), but the latter source is likely located behind the SNR (Nazé et al. 2002). Van der Heyden et al. (2004) analyzed an XMM-Newton observation of the SNR and found that it has a diffuse, center-filled morphology and ISM-like abundances. Van der Heyden et al. (2004) estimated an SNR age of 11 kyr. Due its location close to the H II region NGC 346, Yokogawa

et al. (2002) suggested that this SNR arose from a CC SN, while Sabbi et al. (2007) showed that NGC 346 has evidence of significant SF between 3 and 5 Gyr ago. Based on IKT 18's SFH, we find bursts of SF \sim 40 Myr ago, as well as a sharp peak \lesssim 5 Myr ago that likely is responsible for the birth of NGC 346. Based on our estimates, we expect that 91% of progenitor stars have masses >21.5 M_{\odot} and 9% have masses of 8–12.5 M_{\odot} .

DEM \$108 (B0058-71.8, HFPK 45, SNR J0100.3-7134). Classified as an SNR by Mills et al. (1982) and Mathewson et al. (1984) based on radio and optical observations, this faint SNR was first detected in X-rays using ROSAT (Haberl et al. 2000). Deeper follow-up observations by Filipović et al. (2008) using XMM-Newton found that its X-ray emission is described by a single-temperature, highly absorbed, nonequilibrium ionization plasma. Due to the low X-ray surface brightness of the SNR, Filipović et al. (2008) were unable to constrain the elemental abundances. Filipović et al. (2008) found a welldefined elliptical shell in 6 cm ATCA radio observations that traces the optical shell found in the MCELS (e.g., Winkler et al. 2015). The stellar cluster Bruck 101 (Brueck 1976) is located near the southern rim of the SNR and may be where DEM S108's progenitor star originated. Its SFH exhibits extensive SF activity in the recent past (<50 Myr ago), with an intense burst of metal-rich SF \sim 8–10 Myr ago. Based on our estimates, 100% of the CC progenitors arise from stars of mass $>21.5 M_{\odot}$. Based on a Salpeter IMF, 34% of these stars will have a mass $>40 M_{\odot}$.

IKT 21 (1E 0101.5-7226, HFPK 143, B0101-72.4, SNR J0103.2-7209). This SNR has an incomplete optical and radio shell (Mathewson et al. 1984), and its faint X-ray emission was first discovered using Einstein (Inoue et al. 1983). Follow-up ROSAT observations by Hughes & Smith (1994) found that the SNR's X-ray emission is dominated by the Be pulsar binary system AX J0103-722 (Israel et al. 2000; Haberl & Pietsch 2004). Higher-resolution XMM-Newton observations by van der Heyden et al. (2004) detected faint thermal X-ray emission with a temperature of $kT \sim 0.58 \, \text{keV}$. It is unknown whether AX J0103-722 is associated with the SNR; if so, it would imply that the SNR arose from a CC explosion. The weak X-ray emission of the SNR is associated with enhanced optical ratios that led Hughes & Smith (1994) to suggest that the SNR is expanding into a stellar wind cavity. Similar to IKT 18, IKT 21 is located by the H II region N66. The elemental abundances of the X-ray plasma have not been constrained, so the progenitor mass is currently unknown, although a CC origin is likely, given its proximity to N66 and possible association with a Be/X-ray binary. Similar to IKT 18, the SFH of IKT 21 is dominated by intense, metalrich SF <8 Myr ago, a burst of SF \sim 40 Myr ago, and very little SF prior to then. It is expected that 92% of the progenitor stars have masses $>21.5 M_{\odot}$ and 8% have masses of 8–12.5 M_{\odot} .

HFPK 334 (SNR J0103.5-7247). First detected using ROSAT (Kahabka et al. 1999), HFPK 334 is unusual due to the fact that it emits radio and X-rays (Haberl et al. 2000; Filipović et al. 2008; Crawford et al. 2014) but shows no evidence of optical emission (Payne et al. 2007). Filipović et al. (2008) detected nonthermal, point-like emission at the center of the SNR, which they suggested could be a putative PWN. Follow-up observations by Crawford et al. (2014) confirmed the presence of the point source but found that it was a background object not associated with the SNR. Furthermore,

they found that the SNR's diffuse X-ray emission is best described by a thermal, nonequilibrium ionization plasma model with SMC ISM abundances. Crawford et al. (2014) estimated an age of ~ 1800 yr for the SNR, but they cautioned that the age may be an underestimate because the SNR is expanding into a low-density environment.

1E 0102.2-7219 (DEM S124, IKT 22, B0102-7219, 1E 0102-72.3, HFPK 107, SNR 0102-72.3, SNR J0104.0 -7202). First discovered in X-rays using *Einstein* (Seward & Mitchell 1981), 1E 0102.2-7219 is the brightest SMC SNR in X-rays. Since its discovery, this SNR has been extensively studied in multiple wavelengths. The SNR is oxygen-rich, based on the detection of filamentary [O III] emission (Dopita et al. 1981; Tuohy & Dopita 1983). Hubble Space Telescope observations indicated the presence of O, Ne, and Mg, leading Blair et al. (1989, 2000) to suggest that it is a Type Ib asymmetric, bipolar SN of a 25–35 M_{\odot} Wolf–Rayet star (Vogt & Dopita 2010). Follow-up observations using Spitzer (Stanimirović et al. 2005; Rho et al. 2009), FUSE (Sasaki et al. 2006), XMM-Newton (Sasaki et al. 2006), and Chandra (Gaetz et al. 2000; Davis et al. 2001; Rasmussen et al. 2001; Flanagan et al. 2004; Plucinsky et al. 2017) confirmed the presence of O, Ne, and Mg in the ejecta and found little to no emission from Fe or other heavy elements. Deep Chandra observations have not detected a neutron star (Rutkowski et al. 2010); however, they recently (Vogt et al. 2018) reported the detection of a possible compact central object associated with the remnant that has similar properties to the central compact object of Cas A. Using proper-motion measurements of the X-ray filaments of 1E 0102.2-7219, Hughes et al. (2000) inferred an SNR age of \sim 1000 yr, while Finkelstein et al. (2006) interred an age of \sim 2050 yr from optical filaments. The SNR 1E 0102.2-7219 is in an active star-forming area of the SMC. The SFH is dominated by extensive, metal-rich (Z = 0.008) SF for look-back times >5 Myr. Although uncertain, it is possible that lower-metallicity (Z = 0.004) SF also occurred. Based on Figure 5, the SFH of the vicinity of 1E 0102.2-7219 suggests that 31% of the CC progenitors have a mass of 8–12.5 M_{\odot} , 20% have a mass of 12.5–21.5 M_{\odot} , and 49% have a mass $>21.5\,M_{\odot}$, using a single-star population. Assuming a Salpeter IMF, 69% of the $>21.5 M_{\odot}$ stars would have a mass of 21.5–40 M_{\odot} , so it is possible that the progenitor had a 25-35 M_{\odot} , as suggested by Blair et al. (2000). We also note that significant SF occurred 50–200 Myr ago in the subcell of this source. Assuming a binary stellar population DTD, it is possible that 6% of the stellar population underwent a delayed CC.

IKT 23 $(1E\,0103.3-7240,$ DEM S125, HFPK 217. SNR 0103-72.6, SNR J0105.1-7223). The second-brightest X-ray SNR in the SMC (Seward & Mitchell 1981; Bruhweiler et al. 1987; Cowley et al. 1997; Haberl et al. 2000; van der Heyden et al. 2004), IKT 23 shows a well-defined shell morphology in X-rays (Yokogawa et al. 2002; Park et al. 2003; van der Heyden et al. 2004), and the SNR is faint in the radio (Mills et al. 1982) and optical (Mathewson et al. 1984). This SNR is located close to the H II region DEM S125, and X-ray observations with ASCA (Yokogawa et al. 2002), Chandra (Park et al. 2003), and XMM-Newton (van der Heyden et al. 2004) showed that the SNR has enhanced abundances of O and Ne and marginally enhanced heavier elements compared to SMC ISM abundances. Thus, authors have noted the similarity of IKT 23 with both 1E 0102.2-7219 and the Galactic SNR

G292.0+1.8 (Park et al. 2002). By comparing the elemental abundances of this remnant with Type II SN nucleosynthesis models, Park et al. (2003) suggested that the SNR resulted from a CC of a >18 M_{\odot} progenitor. Similar to 1E 0102.2-7219, the SFH of IKT 23 has significant metal-rich SF at look-back times \gtrsim 10 Myr. Within the uncertainties, there may have been Z=0.004 SF as well, and this SF dominated for earlier lookback times of 1–5 Gyr. The SFR \lesssim 50 Myr ago implies that 100% of the CC SN progenitors in this subcell have masses of 8–12 M_{\odot} , below the \sim 18 M_{\odot} suggested by Park et al. (2003). The vicinity of IKT 23 exhibits substantial SF \gtrsim 50 Myr ago, which, from our analysis, suggests that a significant fraction of the progenitors underwent delayed CC.

DEM S128 (SNR 0103-72.4, B0104-72.2, ITK 24, HFPK 145, SNR J0105.4-7209). First classified as an SNR associated with the H II region of the same name (Inoue et al. 1983), this source has been observed many times in X-rays (Bruhweiler et al. 1987; Wang & Wu 1992; Filipović et al. 2000; Yokogawa et al. 2002; van der Heyden et al. 2004). Follow-up observations in the radio (Filipovic et al. 1997; Filipović et al. 2000, 2005), optical (Filipović et al. 2000; Payne et al. 2007), and infrared (Schwering & Israel 1989) confirmed the SNR classification of the object. Located near the SNR is a Be/X-ray binary, AX J0105-722 (see, e.g., Haberl & Sturm 2016 and references therein). Yokogawa et al. (2002) suggested that the X-ray binary is associated with SNR DEM S128, but other studies indicate it may not be tied to the SNR (Filipović et al. 2000; van der Heyden et al. 2004). The X-ray spectrum of DEM S128 from XMM-Newton observations showed an Fe abundance three times that of the SMC ISM (van der Heyden et al. 2004). This Fe enhancement was confirmed by Roper et al. (2015) using *Chandra* observations. Due to its center-filled X-ray morphology, large optical and radio diameter (Mathewson et al. 1984; Filipović et al. 2000), and enhanced Fe abundance, van der Heyden et al. (2004) and Roper et al. (2015) suggested that the SNR is an old remnant from a Type Ia SN. Details of its SFH are found in Section 5.2.

DEM S130 (SNR J0105.6−7204). Detected as a shell-type SNR in the radio using ACTA and optical (Filipović et al. 2005), this source has not been detected in X-rays (Haberl et al. 2000, 2012a) down to a surface brightness limit of $\sim 10^{-14}$ erg cm⁻² s⁻¹ arcmin⁻². The SNR is a part of the H II region ATCA SMC 444 (J010539−720341; Filipović et al. 2005) and associated with the H II region of the same name (Pellegrini et al. 2012). It is also located near the SNRs IKT 25 and DEM S128. The region's SFH shows an intense burst of SF <50 Myr ago. Thus, DEM S130 is likely from a CC SN. Of the CC progenitors coincident with DEM S130, 76% are stars of mass >21.5 M_{\odot} , while 15% arise from 12.5–21.5 M_{\odot} and 9% arise from 8–21.5 M_{\odot} . Of the >21.5 M_{\odot} progenitors, 34% will have a mass >40 M_{\odot} , assuming a Salpeter IMF.

IKT 25 (B0104–72.3, HFPK 125, SNR 0104–72.3, SNR J0106.2–7205). The fourth-brightest X-ray SNR in the SMC, IKT 25's explosive origin has been debated in the literature. It was discovered in optical wavelengths by Mathewson et al. (1984), and it has been studied extensively in X-rays using ROSAT (Hughes & Smith 1994), XMM-Newton (van der Heyden et al. 2004), Chandra (Lee et al. 2011; Lopez et al. 2014a; Roper et al. 2015), and Suzaku (Takeuchi et al. 2016). It has also been observed in the infrared (Koo et al. 2007), follow-up optical observations (Mathewson et al. 1984; Hughes & Smith 1994; Payne et al. 2007), and

radio (Filipović et al. 2005). The SNR was suggested to arise from a Type Ia SN based on its Balmer-dominated optical spectrum, and Lee et al. (2011) argued that the explosion was a prompt Type Ia explosion in a star-forming region (Koo et al. 2007). Based on enhanced Fe abundances in X-ray observations, van der Heyden et al. (2004) and Roper et al. (2015) also concluded that IKT 25 had a Type Ia origin. However, based on its association with a star-forming region, the detection of a bright IR shell tracing out $H\alpha$ emission, its asymmetric morphology, and its abundance of intermediate-mass elements, other works have claimed it is more consistent with a CC origin (Hughes & Smith 1994; Koo et al. 2007; Lopez et al. 2014a; Takeuchi et al. 2016). Lopez et al. (2014a) noted that Lee et al. (2011) adopted incorrect SMC ISM abundances in their X-ray spectral fits, leading to the mistyping of this source as a Type Ia SNR. Based on their abundance estimates, the SNR's elongated morphology, and the SFH at the site of IKT 25, Lopez et al. (2014a) suggested that the SNR arose from a bipolar Type Ib/ Ic CC SN of an \sim 25 M_{\odot} progenitor. We find that the SFH associated with IKT 25¹² is dominated by intense, metal-rich SF \sim 8 Myr ago that peaked after a steadily increasing SFR since ~ 90 Myr ago. As a result, 76% of the CC SN progenitors associated with IKT 25 are expected to arise from stars of mass $>21.5 M_{\odot}$. Assuming a Salpeter IMF, 69% of the $>21.5 M_{\odot}$ stars would have a mass between 21.5 and $40 M_{\odot}$.

N83C (NS 83, SNR J0114.0-7317, DEM S147, SNR J011333 -731704, B0113-729, SMC B0112-7333, NGC 456, Nail 148, SMC 547, NS 83(A,C)). Very little is known about this SNR. This source was suggested by Filipović et al. (2005) to be a shell-type SNR candidate (ACTA SMC 547) that is possibly interacting with a nearby molecular cloud. Haberl et al. (2012a) detected no X-rays from the position of the source using XMM-Newton, and Temim et al. (2015) showed that the SNR has a high dust-to-gas ratio, indicating that it is in a high-density environment. The SNR N83C is associated with the H II region DEM S147 (Henize 1956; Pellegrini et al. 2012) and located within a bright CO complex in the SMC wing that shows evidence of active SF (e.g., Bolatto et al. 2003). Due to its location close to an active star-forming region and that it is found in a high-density environment (Bolatto et al. 2003; Temim et al. 2015), it is possible that this remnant arises from a CC SN. Its SFH supports this conclusion, with a peak in the SFR \sim 9 Myr ago and limited SF otherwise. We expect that 100% of the CC SN progenitors in this subcell have a mass $>21.5 M_{\odot}$. Adopting a Salpeter IMF, 34% of these stars will have a mass $>40 \, M_{\odot}$.

Appendix B Candidate SNRs

For reference, we list below and in Table 3 candidate SMC SNRs that have been suggested in the literature. We do not include these sources in our analysis, as more detailed follow-up observations are required to confirm their SNR nature.

SXP 1062 SNR. A Be/X-ray binary, SXP 1062 is one of three SMC X-ray pulsars with a pulse period greater than 1000 s. Its optical counterpart is a B0–0.5(III)e+ star (Hénault-Brunet et al. 2012). Hénault-Brunet et al. (2012) discovered faint optical emission surrounding the binary, which

 $[\]overline{^{12}}$ We note that Lopez et al. (2014a) also characterized the SFH of IKT 25, but they selected the wrong subcell (an adjacent one) for this calculation due to a coordinate error. Nonetheless, their conclusion that the SNR likely arose from an ${\sim}25~M_{\odot}$ progenitor still holds.

Table 3
Candidate SNRs Also Suggested in the Literature

Name	R.A.	Decl.	Size (arcmin)
SXP 1062 SNR	01h29m12s	$-73^{\rm d}32^{\rm m}02^{\rm s}$	14
XTE J0111.2-7317	$01^{h}11^{m}09^{s}$	$-73^{d}16^{m}46^{s}$	0.15
NS 66D	$00^{h}57^{m}46^{s}$	$-72^{d}14^{m}04^{s}$	4.8
DEM S25	$00^{h}41^{m}00^{s}$	$-73^{d}36^{m}48^{s}$	1.7
DEM S135	$01^{h}08^{m}20^{s}$	$-71^{d}59^{m}57^{s}$	3.4
XMMU J0049.0-7306	$00^{h}49^{m}00^{s}$	$-73^{d}06^{m}17^{s}$	1.5
XMMU J0056.5-7208	$00^{h}56^{m}30^{s}$	$-72^{d}08^{m}12^{s}$	3.4

they suggested was from an SNR. Using multiwavelength follow-up, Haberl et al. (2012b) confirmed the presence of a shell-type SNR that emits at radio, optical, and X-ray wavelengths. The pulsar is found close to the projected center of this candidate SNR, and Hénault-Brunet et al. (2012) and Haberl et al. (2012b) suggested that the ages of the SNR and SXP 1062 are both <25 kyr. Due to the faintness of the thermal X-ray emission, Haberl et al. (2012b) was unable to constrain the presence of ejecta from this source. The source is near a star-forming region, NGC 602.

 $XTE\ J0111.2\text{-}7317$. Originally discovered as an X-ray pulsar with a 31 s period using RXTE (Chakrabarty et al. 1998a, 1998b), Coe et al. (2000) followed up this source using both optical and IR observations and confirmed that this object is in a Be/X-ray binary with a main-sequence B0–B2 star. From their optical observations, Coe et al. (2000) also found evidence of $H\alpha$ emission, which they suggested is either an SNR or a pulsar wind bow-shock nebula or the H II region. Further follow-up observations seem to suggest that the nebulosity surrounding XTE J0111.2-7317 is likely just an H II region (Coe et al. 2003).

NS 66D (B0056-724, SNR J005800-721101, XMMU J0057.7 -7213, ATCA 345). Located in the southwest bar of the SMC, this source was suggested to be a large (114") SNR by Filipović et al. (2005) and Payne et al. (2007) based on the the radio spectral index derived from ATCA and the detection of radio shell and optical emission. No follow-up observations have been taken to confirm the nature of this source, and it may be associated with the X-ray SNR candidate XMMU J0057.7-7213 suggested by Haberl et al. (2012a).

DEM S25 (DEM S142, N17, SNR J004640-733150, IJL J004643-733112, NGC 265). Similar to NS 66D, this source was suggested to be an SNR based its radio spectral index derived from ATCA (Filipović et al. 2005). However, this source has not been followed up to confirm its SNR origin.

DEM S135 (N80 (80A), S23, SMC B0106-7215, SNR J010819-715956). As with DEM S25 and SN 66D, this source was classified as an SNR candidate by Filipović et al. (2005).

XMMU J0049.0—7306. Discovering it in their X-ray study of the SMC, Haberl et al. (2012a) suggested that this source is an SNR, but no follow-up observations have been taken to confirm the nature of this source.

XMMU J0056.5-7208. Haberl et al. (2012a) discovered this source and suggested that it was an SNR based on detection of thermal X-ray emission. The low count statistics of the XMM-Newton observation precluded constraints on the hot plasma properties of the source. Using MCELS, they confirmed that an

elliptical shell in $H\alpha$ and [SII] is detected. Follow-up observations are needed to confirm the nature of this source.

ORCID iDs

```
Katie Auchettl https://orcid.org/0000-0002-4449-9152
Laura A. Lopez https://orcid.org/0000-0002-1790-3148
Carles Badenes https://orcid.org/0000-0003-3494-343X
Enrico Ramirez-Ruiz https://orcid.org/0000-0003-2558-3102
John F. Beacom https://orcid.org/0000-0002-0005-2631
Tyler Holland-Ashford https://orcid.org/0000-0002-7643-0504
```

References

```
Adams, S. M., & Kochanek, C. S. 2015, MNRAS, 452, 2195
Adams, S. M., Kochanek, C. S., Gerke, J. R., Stanek, K. Z., & Dai, X. 2017,
    MNRAS, 468, 4968
Anderson, J. P., & James, P. A. 2008, MNRAS, 390, 1527
Anderson, J. P., James, P. A., Förster, F., et al. 2015, MNRAS, 448, 732
Antoniou, V., Zezas, A., Hatzidimitriou, D., & Kalogera, V. 2010, ApJL,
Aubourg, É., Tojeiro, R., Jimenez, R., et al. 2008, A&A, 492, 631
Auchettl, K., Slane, P., Castro, D., Foster, A. R., & Smith, R. K. 2015, ApJ,
  810, 43
Badenes, C., Borkowski, K. J., Hughes, J. P., Hwang, U., & Bravo, E. 2006,
   ApJ, 645, 1373
Badenes, C., Harris, J., Zaritsky, D., & Prieto, J. L. 2009, ApJ, 700, 727
Badenes, C., Hughes, J. P., Cassam-Chenaï, G., & Bravo, E. 2008, ApJ,
  680, 1149
Badenes, C., Maoz, D., & Draine, B. T. 2010, MNRAS, 407, 1301
Bastian, N., Cabrera-Ziri, I., Niederhofer, F., et al. 2017, MNRAS, 465, 4795
Bastian, N., Covey, K. R., & Meyer, M. R. 2010, ARA&A, 48, 339
Bate, M. R., & Bonnell, I. A. 2005, MNRAS, 356, 1201
Bekki, K., & Chiba, M. 2005, MNRAS, 356, 680
Bekki, K., Couch, W. J., Beasley, M. A., et al. 2004, ApJL, 610, L93
Bersten, M. C., Benvenuto, O. G., Folatelli, G., et al. 2014, AJ, 148, 68
Besla, G., Kallivayalil, N., Hernquist, L., et al. 2012, MNRAS, 421, 2109
Bica, E. L. D., & Schmitt, H. R. 1995, ApJS, 101, 41
Blair, W. P., Ghavamian, P., Long, K. S., et al. 2007, ApJ, 662, 998
Blair, W. P., Morse, J. A., Raymond, J. C., et al. 2000, ApJ, 537, 667
Blair, W. P., Raymond, J. C., Danziger, J., & Matteucci, F. 1989, ApJ,
  338, 812
Blondin, J. M., Wright, E. B., Borkowski, K. J., & Reynolds, S. P. 1998, ApJ,
  500, 342
Bolatto, A. D., Leroy, A., Israel, F. P., & Jackson, J. M. 2003, ApJ, 595, 167
Bolatto, A. D., Leroy, A. K., Jameson, K., et al. 2011, ApJ, 741, 12
Bonnell, I. A., Bate, M. R., & Zinnecker, H. 1998, MNRAS, 298, 93
Bouret, J.-C., Lanz, T., Martins, F., et al. 2013, A&A, 555, A1
Bromm, V., & Larson, R. B. 2004, ARA&A, 42, 79
Brott, I., de Mink, S. E., Cantiello, M., et al. 2011, A&A, 530, A115
Brueck, M. T. 1976, ORROE, 1, 1
Bruhweiler, F. C., Klinglesmith, D. A., III, Gull, T. R., & Sofia, S. 1987, ApJ,
  317, 152
Burkey, M. T., Reynolds, S. P., Borkowski, K. J., & Blondin, J. M. 2013, ApJ,
Cao, Y., Kasliwal, M. M., Arcavi, I., et al. 2013, ApJL, 775, L7
Casetti-Dinescu, D. I., Moni Bidin, C., Girard, T. M., et al. 2014, ApJL,
   784, L37
Chakrabarty, D., Levine, A. M., Clark, G. W., & Takeshima, T. 1998a,
  IAUC, 7048
Chakrabarty, D., Takeshima, T., Ozaki, M., Paul, B., & Yokogawa, J. 1998b,
  IAUC, 7062
Chevalier, R. A. 1982, ApJ, 258, 790
Chevalier, R. A. 2005, ApJ, 619, 839
Chevalier, R. A., & Oishi, J. 2003, ApJL, 593, L23
Choi, J., Dotter, A., Conroy, C., et al. 2016, ApJ, 823, 102
Chomiuk, L., & Wilcots, E. M. 2009, ApJ, 703, 370
Coe, M. J., Haigh, N. J., & Reig, P. 2000, MNRAS, 314, 290
Coe, M. J., Haigh, N. J., Wilson, C. A., & Negueruela, I. 2003, MNRAS,
  344, 1075
Couch, S. M., & Ott, C. D. 2015, ApJ, 799, 5
Cowley, A. P., Schmidtke, P. C., McGrath, T. K., et al. 1997, PASP, 109, 21
```

```
Crawford, E. J., Filipović, M. D., McEntaffer, R. L., et al. 2014, AJ, 148, 99
Da Costa, G. S., & Hatzidimitriou, D. 1998, AJ, 115, 1934
Dabringhausen, J., Kroupa, P., Pflamm-Altenburg, J., & Mieske, S. 2012, ApJ,
Dan, M., Rosswog, S., Guillochon, J., & Ramirez-Ruiz, E. 2011, ApJ, 737, 89
D'Antona, F., Di Criscienzo, M., Decressin, T., et al. 2015, MNRAS,
   453, 2637
Davis, D. S., Flanagan, K. A., Houck, J. C., et al. 2001, in AIP Conf. Ser. 565,
   Young Supernova Remnants, ed. S. S. Holt & U. Hwang (Melville, NY:
   AIP), 230
De Donder, E., & Vanbeveren, D. 1998, A&A, 333, 557
de Mink, S. E., Brott, I., Cantiello, M., et al. 2012, in ASP Conf. Ser. 465, Proc.
   Scientific Meeting in Honor of Anthony F.J. Moffat, ed. L. Drissen et al.
   (San Francisco, CA: ASP), 65
de Mink, S. E., Langer, N., Izzard, R. G., Sana, H., & de Koter, A. 2013, ApJ,
   764, 166
de Mink, S. E., Sana, H., Langer, N., Izzard, R. G., & Schneider, F. R. N. 2014,
     pJ, 782, 7
de Plaa, J., Werner, N., Bleeker, J. A. M., et al. 2007, A&A, 465, 345
Di Matteo, P., Haywood, M., Combes, F., Semelin, B., & Snaith, O. N. 2013,
     &A, 553, A102
Diaz, J., & Bekki, K. 2011, MNRAS, 413, 2015
Díaz-Rodríguez, M., Murphy, J. W., Rubin, D. A., et al. 2018, ApJ, 861, 92
Dickel, J. R., Williams, R. M., Carter, L. M., et al. 2001, AJ, 122, 849
Dolence, J. C., Burrows, A., & Zhang, W. 2015, ApJ, 800, 10
Dolphin, A. E., Walker, A. R., Hodge, P. W., et al. 2001, ApJ, 562, 303
D'Onghia, E., & Fox, A. J. 2016, ARA&A, 54, 363
Dopita, M. A., Tuohy, I. R., & Mathewson, D. S. 1981, ApJL, 248, L105
Dopita, M. A. 1991, in IAU Symp. 148, The Magellanic Clouds, ed.
  R. Haynes & D. Milne (Dordrecht: Kluwer), 393
Douna, V. M., Pellizza, L. J., Mirabel, I. F., & Pedrosa, S. E. 2015, A&A,
  579, A44
Dray, L. M. 2006, MNRAS, 370, 2079
Dray, L. M., & Tout, C. A. 2007, MNRAS, 376, 61
Dufour, R. J. 1984, IAUS, 108, 353
Dupree, A. K., Dotter, A., Johnson, C. I., et al. 2017, ApJL, 846, L1
Ebinger, K., Curtis, S., Fröhlich, C., et al. 2018, arXiv:1804.03182
El-Badry, K., Wetzel, A., Geha, M., et al. 2016, ApJ, 820, 131
Eldridge, J. J., Fraser, M., Maund, J. R., & Smartt, S. J. 2015, MNRAS,
   446, 2689
Eldridge, J. J., Fraser, M., Smartt, S. J., Maund, J. R., & Crockett, R. M. 2013,
   MNRAS, 436, 774
Eldridge, J. J., Izzard, R. G., & Tout, C. A. 2008, MNRAS, 384, 1109
Eldridge, J. J., Langer, N., & Tout, C. A. 2011, MNRAS, 414, 3501
Eldridge, J. J., Stanway, E. R., Xiao, L., et al. 2017, PASA, 34, e058
Eldridge, J. J., & Tout, C. A. 2004, MNRAS, 353, 87
Filipović, M. D., Haberl, F., Pietsch, W., & Morgan, D. H. 2000, A&A,
   353, 129
Filipović, M. D., Haberl, F., Winkler, P. F., et al. 2008, A&A, 485, 63
Filipovic, M. D., Jones, P. A., White, G. L., et al. 1997, A&AS, 121, 321
Filipović, M. D., Payne, J. L., Reid, W., et al. 2005, MNRAS, 364, 217
Filipovic, M. D., Pietsch, W., Haynes, R. F., et al. 1998, A&AS, 127, 119
Finkelstein, S. L., Morse, J. A., Green, J. C., et al. 2006, ApJ, 641, 919
Flanagan, K. A., Canizares, C. R., Dewey, D., et al. 2004, ApJ, 605, 230
Fox, O. D., Van Dyk, S. D., Dwek, E., et al. 2017, ApJ, 836, 222
Fryer, C. L., Belczynski, K., Wiktorowicz, G., et al. 2012, ApJ, 749, 91
Gaetz, T. J., Butt, Y. M., Edgar, R. J., et al. 2000, ApJL, 534, L47
Galbany, L., Stanishev, V., Mourão, A. M., et al. 2014, A&A, 572, A38
Gal-Yam, A. 2017, Handbook of Supernovae (Berlin: Springer), 195
Geha, M., Brown, T. M., Tumlinson, J., et al. 2013, ApJ, 771, 29
Gelfand, J. D., Slane, P. O., & Temim, T. 2015, ApJ, 807, 30
Gerke, J. R., Kochanek, C. S., & Stanek, K. Z. 2015, MNRAS, 450, 3289
Golden-Marx, J. B., Oey, M. S., Lamb, J. B., & Graus, A. S. 2014,
   arXiv:1411.3185
González-Casanova, D. F., De Colle, F., Ramirez-Ruiz, E., & Lopez, L. A.
   2014, ApJL, 781, L26
Guillochon, J., Dan, M., Ramirez-Ruiz, E., & Rosswog, S. 2010, ApJL,
   709. L64
Haberl, F., Filipović, M. D., Pietsch, W., & Kahabka, P. 2000, A&AS, 142, 41
Haberl, F., & Pietsch, W. 2004, A&A, 414, 667
Haberl, F., & Sturm, R. 2016, A&A, 586, A81
Haberl, F., Sturm, R., Ballet, J., et al. 2012a, A&A, 545, A128
Haberl, F., Sturm, R., Filipović, M. D., Pietsch, W., & Crawford, E. J. 2012b,
    &A, 537, L1
Hachisu, I., Kato, M., & Nomoto, K. 1996, ApJL, 470, L97
```

Han, Z., & Podsiadlowski, P. 2004, MNRAS, 350, 1301

```
Harris, J., & Zaritsky, D. 2001, ApJS, 136, 25
Harris, J., & Zaritsky, D. 2004, AJ, 127, 1531
Harris, J., & Zaritsky, D. 2009, AJ, 138, 1243
Heger, A., Fryer, C. L., Woosley, S. E., Langer, N., & Hartmann, D. H. 2003,
   AnJ. 591, 288
Hénault-Brunet, V., Oskinova, L. M., Guerrero, M. A., et al. 2012, MNRAS,
  420, L13
Hendrick, S. P., Reynolds, S. P., & Borkowski, K. J. 2005, ApJL, 622, L117
Henize, K. G. 1956, ApJS, 2, 315
Hilditch, R. W., Howarth, I. D., & Harries, T. J. 2005, MNRAS, 357, 304
Hirschi, R. 2007, A&A, 461, 571
Hirschi, R., Meynet, G., & Maeder, A. 2005, A&A, 443, 581
Holoien, T. W.-S., Brown, J. S., Stanek, K. Z., et al. 2017, MNRAS, 471, 4966
Hughes, J. P., Rakowski, C. E., & Decourchelle, A. 2000, ApJL, 543, L61
Hughes, J. P., & Smith, R. C. 1994, AJ, 107, 1363
Hunter, I., Lennon, D. J., Dufton, P. L., et al. 2008, A&A, 479, 541
Hunter, I., Lennon, D. J., Dufton, P. L., et al. 2009, A&A, 504, 211
Ibeling, D., & Heger, A. 2013, ApJL, 765, L43
Iben, I., Jr. 1974, ARA&A, 12, 215
Iben, I., Jr., & Tutukov, A. V. 1984, ApJS, 54, 335
Inoue, H., Koyama, K., & Tanaka, Y. 1983, in IAU Symp. 101, Supernova
   Remnants and their X-ray Emission, ed. J. Danziger & P. Gorenstein
   (Dordrecht: Reidel), 535
Israel, G. L., Campana, S., Covino, S., et al. 2000, ApJL, 531, L131
Izzard, R. G., Ramirez-Ruiz, E., & Tout, C. A. 2004, MNRAS, 348, 1215
James, P. A., & Anderson, J. P. 2006, A&A, 453, 57
Janka, H.-T. 2017, Handbook of Supernovae (Berlin: Springer), 1095
Jennings, Z. G., Williams, B. F., Murphy, J. W., et al. 2012, ApJ, 761, 26
Jennings, Z. G., Williams, B. F., Murphy, J. W., et al. 2014, ApJ, 795, 170
Kahabka, P., Pietsch, W., Filipović, M. D., & Haberl, F. 1999, A&AS, 136, 81
Kallivayalil, N., van der Marel, R. P., Besla, G., Anderson, J., & Alcock, C.
   2013, ApJ, 764, 161
Kilpatrick, C. D., Takaro, T., Foley, R. J., et al. 2018, MNRAS, 480, 2072
Kippenhahn, R., & Weigert, A. 1967, ZAp, 65, 251
Kistler, M. D., Stanek, K. Z., Kochanek, C. S., Prieto, J. L., & Thompson, T. A.
   2013, ApJ, 770, 88
Kobayashi, C., Tsujimoto, T., Nomoto, K., Hachisu, I., & Kato, M. 1998,
    pJL, 503, L155
Kochanek, C. S., Fraser, M., Adams, S. M., et al. 2017, MNRAS, 467, 3347
Koo, B.-C., Lee, H.-G., Moon, D.-S., et al. 2007, PASJ, 59, S455
Korn, A. J., Becker, S. R., Gummersbach, C. A., & Wolf, B. 2000, A&A,
  353, 655
Koyama, K., Kinugasa, K., Matsuzaki, K., et al. 1997, PASJ, 49, L7
Koyama, K., Petre, R., Gotthelf, E. V., et al. 1995, Natur, 378, 255
Krause, O., Birkmann, S. M., Usuda, T., et al. 2008, Sci, 320, 1195
Langer, N. 1998, A&A, 329, 551
Langer, N., Deutschmann, A., Wellstein, S., & Höflich, P. 2000, A&A,
   362, 1046
Larson, R. B. 2005, MNRAS, 359, 211
Lee, J.-J., Park, S., Hughes, J. P., Slane, P. O., & Burrows, D. N. 2011, ApJL,
  731, L8
Lee, M.-Y., Stanimirović, S., Ott, J., et al. 2009, AJ, 138, 1101
Lewis, A. R., Dolphin, A. E., Dalcanton, J. J., et al. 2015, ApJ, 805, 183
Li, W., Leaman, J., Chornock, R., et al. 2011, MNRAS, 412, 1441
Lopez, L. A., Castro, D., Slane, P. O., Ramirez-Ruiz, E., & Badenes, C. 2014a,
   ApJ, 788, 5
Lopez, L. A., Krumholz, M. R., Bolatto, A. D., et al. 2014b, ApJ, 795, 121
Lopez, L. A., Ramirez-Ruiz, E., Badenes, C., et al. 2009a, ApJL, 706, L106
Lopez, L. A., Ramirez-Ruiz, E., Castro, D., & Pearson, S. 2013, ApJ, 764, 50
Lopez, L. A., Ramirez-Ruiz, E., Huppenkothen, D., Badenes, C., &
   Pooley, D. A. 2011, ApJ, 732, 114
Lopez, L. A., Ramirez-Ruiz, E., Pooley, D. A., & Jeltema, T. E. 2009b, ApJ,
   691, 875
Maeda, K., & Terada, Y. 2016, IJMPD, 25, 1630024
Maeder, A., & Meynet, G. 2000, ARA&A, 38, 143
Maggi, P., Haberl, F., Kavanagh, P. J., et al. 2016, A&A, 585, A162
Maitra, C., Ballet, J., Filipović, M. D., et al. 2015, A&A, 584, A41
Maoz, D., & Badenes, C. 2010, MNRAS, 407, 1314
Maoz, D., & Graur, O. 2017, ApJ, 848, 25
Maoz, D., & Mannucci, F. 2012, PASA, 29, 447
Maoz, D., Mannucci, F., & Brandt, T. D. 2012, MNRAS, 426, 3282
Maoz, D., Mannucci, F., Li, W., et al. 2011, MNRAS, 412, 1508
Maoz, D., Mannucci, F., & Nelemans, G. 2014, ARA&A, 52, 107
Marks, M., Kroupa, P., Dabringhausen, J., & Pawlowski, M. S. 2012,
  MNRAS, 422, 2246
Martayan, C., Frémat, Y., Hubert, A.-M., et al. 2007, A&A, 462, 683
```

```
Martínez-Rodríguez, H., Piro, A. L., Schwab, J., & Badenes, C. 2016, ApJ,
Martín-Navarro, I., Vazdekis, A., La Barbera, F., et al. 2015, ApJL, 806, L31
Massey, P., Parker, J. W., & Garmany, C. D. 1989, AJ, 98, 1305
Mathewson, D. S., Ford, V. L., Dopita, M. A., et al. 1984, ApJS, 55, 189
Maund, J. R. 2017, MNRAS, 469, 2202
Maund, J. R. 2018, MNRAS, 476, 2629
McKee, C. F. 1974, ApJ, 188, 335
McKee, C. F., & Ostriker, J. P. 1977, ApJ, 218, 148
Meng, X., Chen, X., & Han, Z. 2008, A&A, 487, 625
Milisavljevic, D., & Fesen, R. A. 2017, Handbook of Supernovae (Berlin:
   Springer), 2211
Mills, B. Y., Little, A. G., Durdin, J. M., & Kesteven, M. J. 1982, MNRAS,
   200, 1007
Milone, A. P., Marino, A. F., D'Antona, F., et al. 2016, MNRAS, 458,
   4368
Mokiem, M. R., de Koter, A., Vink, J. S., et al. 2007, A&A, 473, 603
Müller, B. 2016, PASA, 33, e048
Murphy, J. W., Dolence, J. C., & Burrows, A. 2013, ApJ, 771, 52
Nazé, Y., Hartwell, J. M., Stevens, I. R., et al. 2002, ApJ, 580, 225
Nomoto, K., Hashimoto, M., Tsujimoto, T., et al. 1997, NuPhA, 616, 79
Olszewski, E. W., Schommer, R. A., Suntzeff, N. B., & Harris, H. C. 1991, AJ,
   101, 515
Owen, R. A., Filipović, M. D., Ballet, J., et al. 2011, A&A, 530, A132
Padoan, P., & Nordlund, A. 2002, ApJ, 576, 870
Pagel, B. E. J., & Tautvaišienė, G. 1999, Ap&SS, 265, 461
Park, S., & Bhalerao, J. 2017, ApJ, 834, 189
Park, S., Hughes, J. P., Burrows, D. N., et al. 2003, ApJL, 598, L95
Park, S., Hughes, J. P., Slane, P. O., et al. 2004, ApJL, 602, L33
Park, S., Roming, P. W. A., Hughes, J. P., et al. 2002, ApJL, 564, L39
Patnaude, D. J., Lee, S.-H., Slane, P. O., et al. 2015, ApJ, 803, 101
Payne, J. L., Filipović, M. D., Reid, W., et al. 2004, MNRAS, 355, 44
Payne, J. L., White, G. L., Filipović, M. D., & Pannuti, T. G. 2007, MNRAS,
Pejcha, O., & Thompson, T. A. 2015, ApJ, 801, 90
Pellegrini, E. W., Oey, M. S., Winkler, P. F., et al. 2012, ApJ, 755, 40
Piatti, A. E., Santos, J. F. C., Clariá, J. J., et al. 2001, MNRAS, 325, 792
Piatti, A. E., Sarajedini, A., Geisler, D., Seguel, J., & Clark, D. 2005, MNRAS,
   358, 1215
Plucinsky, P., Sharda, P., Gaetz, T., & Kashyap, V. 2018, AAS Meeting, 231,
Plucinsky, P. P., Beardmore, A. P., Foster, A., et al. 2017, A&A, 597, A35
Pols, O. R., Schröder, K.-P., Hurley, J. R., Tout, C. A., & Eggleton, P. P. 1998,
        AS, 298, 525
Prieto, J. L., Stanek, K. Z., & Beacom, J. F. 2008, ApJ, 673, 999
Ramirez-Ruiz, E., Lazzati, D., & Blain, A. W. 2002, ApJL, 565, L9
Rasmussen, A. P., Behar, E., Kahn, S. M., den Herder, J. W., &
   van der Heyden, K. 2001, A&A, 365, L231
Renzo, M., Zapartas, E., de Mink, S. E., et al. 2018, arXiv:1804.09164
Rest, A., Matheson, T., Blondin, S., et al. 2008a, ApJ, 680, 1137
Rest, A., Suntzeff, N. B., Olsen, K., et al. 2005, Natur, 438, 1132
Rest, A., Welch, D. L., Suntzeff, N. B., et al. 2008b, ApJL, 681, L81
Reynolds, S. P., Borkowski, K. J., Hwang, U., et al. 2007, ApJL, 668, L135
Rho, J., Reach, W. T., Tappe, A., et al. 2009, ApJ, 700, 579
Roper, Q., McEntaffer, R. L., DeRoo, C., et al. 2015, ApJ, 803, 106
Roškar, R., Debattista, V. P., Quinn, T. R., & Wadsley, J. 2012, MNRAS,
Russell, S. C., & Dopita, M. A. 1992, ApJ, 384, 508
Rutkowski, M. J., Schlegel, E. M., Keohane, J. W., & Windhorst, R. A. 2010,
   ApJ, 715, 908
Sabbi, E., Sirianni, M., Nota, A., et al. 2007, AJ, 133, 44
Salpeter, E. E. 1955, ApJ, 121, 161
Sana, H., de Mink, S. E., de Koter, A., et al. 2012, Sci, 337, 444
Sarbadhicary, S. K., Badenes, C., Chomiuk, L., Caprioli, D., & Huizenga, D.
  2017, MNRAS, 464, 2326
Sasaki, M., Gaetz, T. J., Blair, W. P., et al. 2006, ApJ, 642, 260
Sato, K., Tokoi, K., Matsushita, K., et al. 2007, ApJL, 667, L41
Schenck, A., Park, S., Burrows, D. N., et al. 2014, ApJ, 791, 50
Schneider, F. R. N., Izzard, R. G., de Mink, S. E., et al. 2014, ApJ, 780, 117
```

```
Schneider, F. R. N., Izzard, R. G., Langer, N., & de Mink, S. E. 2015, ApJ,
  805, 20
Schneider, R., Ferrara, A., Natarajan, P., & Omukai, K. 2002, ApJ, 571, 30
Schroyen, J., De Rijcke, S., Koleva, M., Cloet-Osselaer, A., &
  Vandenbroucke, B. 2013, MNRAS, 434, 888
Schwering, P. B. W., & Israel, F. P. 1989, A&AS, 79, 79
Sedov, L. I. 1959, Similarity and Dimensional Methods in Mechanics (New
   York: Academic)
Sellwood, J. A., & Binney, J. J. 2002, MNRAS, 336, 785
Seward, F. D., & Mitchell, M. 1981, ApJ, 243, 736
Shtykovskiy, P., & Gilfanov, M. 2005, MNRAS, 362, 879
Sim, S. A., Röpke, F. K., Hillebrandt, W., et al. 2010, ApJL, 714, L52
Skibba, R. A., Engelbracht, C. W., Aniano, G., et al. 2012, ApJ, 761, 42
Slane, P., Gaensler, B. M., Dame, T. M., et al. 1999, ApJ, 525, 357
Smartt, S. J. 2009, ARA&A, 47, 63
Smartt, S. J. 2015, PASA, 32, e016
Smartt, S. J., Eldridge, J. J., Crockett, R. M., & Maund, J. R. 2009, MNRAS,
  395, 1409
Smith, R. C. & MCELS Team 1999, in IAU Symp. 190, New Views of the
  Magellanic Clouds, ed. Y.-H. Chu et al. (Dordrecht: Kluwer), 28
Sreenivasan, S. R., & Wilson, W. J. F. 1982, ApJ, 254, 287
Stanimirović, S., Bolatto, A. D., Sandstrom, K., et al. 2005, ApJL, 632, L103
Stanimirović, S., Staveley-Smith, L., & Jones, P. A. 2004, ApJ, 604, 176
Sterken, C., & Breysacher, J. 1997, A&A, 328, 269
Stinson, G. S., Dalcanton, J. J., Quinn, T., et al. 2009, MNRAS, 395, 1455
Sukhbold, T., Ertl, T., Woosley, S. E., Brown, J. M., & Janka, H.-T. 2016, ApJ,
Sukhbold, T., & Woosley, S. E. 2014, ApJ, 783, 10
Sullivan, M., Le Borgne, D., Pritchet, C. J., et al. 2006, ApJ, 648, 868
Takeuchi, Y., Yamaguchi, H., & Tamagawa, T. 2016, PASJ, 68, S9
Taylor, G. 1950, RSPSA, 201, 159
Temim, T., Dwek, E., Tchernyshyov, K., et al. 2015, ApJ, 799, 158
Temim, T., Slane, P., Reynolds, S. P., Raymond, J. C., & Borkowski, K. J.
   2010, ApJ, 710, 309
Thompson, T. A., Quataert, E., & Burrows, A. 2005, ApJ, 620, 861
Truelove, J. K., & McKee, C. F. 1999, ApJS, 120, 299
Tsujimoto, T., Nomoto, K., Yoshii, Y., et al. 1995, MNRAS, 277, 945
Tuohy, I. R., & Dopita, M. A. 1983, ApJL, 268, L11
Ugliano, M., Janka, H.-T., Marek, A., & Arcones, A. 2012, ApJ, 757, 69
Umeda, H., Nomoto, K., Yamaoka, H., & Wanajo, S. 1999, ApJ, 513, 861
van der Heyden, K. J., Bleeker, J. A. M., & Kaastra, J. S. 2004, A&A, 421, 1031
Van Dyk, S. D., Zheng, W., Brink, T. G., et al. 2018, ApJ, 860, 90
van Kerkwijk, M. H., Chang, P., & Justham, S. 2010, ApJL, 722, L157
Vink, J. 2012, A&ARv, 20, 49
Vink, J. S., de Koter, A., & Lamers, H. J. G. L. M. 2001, A&A, 369, 574
Vogt, F., & Dopita, M. A. 2010, ApJ, 721, 597
Vogt, F. P. A., Bartlett, E. S., Seitenzahl, I. R., et al. 2018, NatAs, 2, 465
Wang, Q., & Wu, X. 1992, ApJS, 78, 391
Wang, X., Wang, L., Filippenko, A. V., Zhang, T., & Zhao, X. 2013, Sci,
  340, 170
Warren, J. S., & Hughes, J. P. 2004, ApJ, 608, 261
Weidner, C., Kroupa, P., & Maschberger, T. 2009, MNRAS, 393, 663
Wilke, K., Klaas, U., Lemke, D., et al. 2004, A&A, 414, 69
Williams, B. F., Peterson, S., Murphy, J., et al. 2014a, ApJ, 791, 105
Williams, B. J., Borkowski, K. J., Reynolds, S. P., et al. 2014b, ApJ, 790, 139
Williams, R. N., Chu, Y. H., Chen, C. H., et al. 2006, BAAS, 38, 1114
Winkler, P. F., Smith, R. C., Points, S. D. & MCELS Team 2015, in ASP Conf.
  Ser. 491, Fifty Years of Wide Field Studies in the Southern Hemisphere:
  Resolved Stellar Populations of the Galactic Bulge and Magellanic Clouds,
  ed. S. Points & A. Kunder (San Francisco, CA: ASP), 343
Wongwathanarat, A., Müller, E., & Janka, H.-T. 2015, A&A, 577, A48
Woosley, S. E., Heger, A., & Weaver, T. A. 2002, RvMP, 74, 1015
Yamaguchi, H., Badenes, C., Foster, A. R., et al. 2015, ApJL, 801, L31
Yokogawa, J., Imanishi, K., Koyama, K., Nishiuchi, M., & Mizuno, N. 2002,
    ASJ, 54, 53
Yokogawa, J., Torii, K., Imanishi, K., & Koyama, K. 2000, PASJ, 52, L37
Zapartas, E., de Mink, S. E., Izzard, R. G., et al. 2017, arXiv:1701.07032
Zaritsky, D., Harris, J., Thompson, I. B., Grebel, E. K., & Massey, P. 2002, AJ,
```

123, 855